Biological Time Equivalence in Vertebrates: Thermodynamic Framework, Comparative Tests, and Clade-Specific Deviations

Mesfin Asfaw Taye

West Los Angeles College, Science Division 9000 Overland Ave, Culver City, CA 90230, USA
tayem@wlac.edu

DOI: 10.29322/IJSRP.16.05.2026.p17307
https://dx.doi.org/10.29322/IJSRP.16.05.2026.p17307

Paper Received Date: 14th March 2026
Paper Acceptance Date: 19th April 2026
Paper Publication Date: 8th May 2026

Abstract

Across adult warm-blooded vertebrates, the product of resting heart rate f_H and maximum lifespan L is approximately constant: $N_* = f_H\, L \approx 10^9$ cardiac cycles. This empirical regularity, noted since Rubner (1908), has lacked a widely accepted thermodynamic interpretation. We derive $N_* \approx 10^9$ from the non-equilibrium second law by treating the adult organism as a metabolic non-equilibrium steady state (NESS) and introducing the empirical closure $\dot{e}_p = \sigma_O f$, which links entropy production rate to heart rate via a mass-specific parameter $\sigma_O \propto M^{\circ}$. Under this closure, the lifetime entropy budget $\Sigma = \sigma_O N_*$ is approximately species-independent when σ_O is approximately constant—a condition whose direct calorimetric verification remains the critical outstanding experimental test. We further show that N_* is the correct primitive invariant: lifetime energy per unit mass is a derived consequence, valid only when body temperature and the mass-specific entropy cost per cycle are both approximately constant. This framework, which we term the Principle of Biological Time Equivalence (PBTE), is placed on a fully falsifiable footing with explicit assumptions, a domain-of-validity table, and five numerical falsification criteria. We test the framework against a dataset of 230 adult vertebrate species spanning eight taxonomic groups. Ordinary least-squares regression on the $n = 43$ directly measured non-primate placentals yields slope $\hat{\beta} = -0.903 \pm 0.056$ ($R^2 = 0.863$; F-test $p = 0.093$ against $\beta = -1$). Phylogenetically independent contrasts on 112 endotherm species yield a $\log_{10} f_H$–$\log_{10} L$ slope of -0.99 ± 0.04 ($p = 0.84$ against slope -1), confirming the relation is not a phylogenetic artefact. The WBE kinematic null of zero inter-clade variation is rejected ($F = 12.7$, $p < 0.001$). Four warm-blooded clades depart systematically from the mammalian baseline; we derive their longevity deviations from a unified thermodynamic multiplier $\Phi_C = \Phi_{duty} \cdot \Phi_{thermal} \cdot \Phi_{mito+oxid} \cdot \Phi_{haz}$, calibrated to independently measured physiology. For primates, the elevated count $\langle N_* \rangle \approx (2\text{–}3) \times 10^9$ follows from a neuro-metabolic entropy model in which greater neural metabolic investment reduces entropy produced per cardiac cycle. For bats, the extreme longevity ($\Phi_{bat} \approx 7.9$) arises from the multiplicative synergy of cardiac suppression during torpor and an Arrhenius thermal factor during hibernation—two mechanisms acting simultaneously whose thermodynamic motivation has not previously been given. For birds, an adverse thermal penalty ($\Phi_{thermal} = 0.73$) and adverse flight duty cycle ($\Phi_{duty} = 0.87$) are overcome by mitochondrial coupling efficiency and

antioxidant robustness. For cetaceans, extreme diving bradycardia ($\Phi_{duty} = 3.08$ for bowhead whales) reveals a near-coincidence trap: the raw heartbeat count $N_{obs} \approx N_O$ conceals a true thermodynamic budget three times the mammalian baseline. Within this framework, the integral of physiological frequency defines a natural biological proper time, which unifies all longevity

mechanisms as Class 1 (time dilation: reduce f) or Class 2 (budget expansion: reduce σ_0), generating testable predictions for epigenetic aging clocks. The central outstanding experimental requirement is direct calorimetric verification of $\sigma_0 \propto M^0$, which would convert PBTE from a statistically supported regularity with thermodynamic motivation into a fully tested conservation law.

Keywords: metabolic scaling, biological time, non-equilibrium thermodynamics, lifespan invariant, allometry, entropy production, comparative physiology, clade multiplier, epigenetic clock, falsifiability

Contents

1 Introduction

Among the most arresting regularities in comparative biology is one that spans the full breadth of vertebrate life: a pygmy shrew (*Suncus etruscus*, $\approx$ 2 g) races through existence at 835 heartbeats per minute and dies within two years; an African elephant ($\approx$ 4,000 kg) beats its heart at a leisurely 28 beats per minute and endures for seven decades. To an observer measuring time by the calendar, their lifespans differ by a factor of thirty-five. Yet when duration is measured not by years but by the organism's own internal rhythm—the cumulative count of cardiac cycles—the two animals are, in a deeper sense, contemporaries. Each accumulates close to 10^9 heartbeats before death, so that

$$N = f_{\mathrm{H}} \cdot L \approx 835\,\mathrm{min}^{-1} \times 2\,\mathrm{yr} \approx 28\,\mathrm{min}^{-1} \times 70\,\mathrm{yr} \approx 10^9, \tag{1}$$

where f_{H} is the resting heart rate and L is the maximum lifespan. This near-equality, first noted through the constancy of mass-specific lifetime energy expenditure by Rubner [1] and later quantified as a universal temporal allometry by Lindstedt and Calder [2]—with the heartbeat count itself explicitly computed by Livingstone and Kuehn [3] and Levine [4]—has accumulated substantial empirical support across body masses spanning ten orders of magnitude. It is captured by the dimensionless invariant

$$\ell_{\mathrm{i}} \equiv \log_{10} f_{\mathrm{H,i}} \cdot L_{\mathrm{i}} \cdot 525{,}960 \approx 9.06, \tag{2}$$

where 525,960 min yr^{-1} is the conversion factor, and equivalently $N_\star = f_{\mathrm{H,i}}\, L_{\mathrm{i}} \cdot 525{,}960 \approx 10^9$ cardiac cycles per lifetime.

The constancy of $N_\star$ is not merely a numerical curiosity: it points toward a fundamental organising principle of animal physiology. Organisms do not age primarily by elapsed chronological time, but by the accumulation of irreversible physiological events. Just as Einstein's special relativity teaches that proper time is intrinsic to an observer and cannot be inferred from an external clock [5], biological time is intrinsic to each organism. A hummingbird's minute is dense with metabolic activity and entropy production; a tortoise's minute is comparatively sparse; yet both traverse, in their own internal frames, a comparable extent of biological duration before reaching the same thermodynamic endpoint. Chronological lifespan is thus an emergent consequence of how rapidly an organism spends its fixed biological time budget—not the budget itself.

What makes this regularity scientifically compelling—and scientifically challenging—is that it holds only approximately, and its deviations are not random. Certain clades depart from the mammalian baseline in striking and consistent ways. Primates, including humans, accumulate $(2\text{–}3) \times 10^9$ heartbeats over a lifetime, roughly twice the baseline. This elevation is not explained by slower heart rates alone; rather, it reflects a fundamental reduction in the thermodynamic cost of each cardiac cycle, driven by the extraordinary metabolic investment that primates make in their neural tissue. A large, metabolically active brain provides enhanced predictive homeostatic control over peripheral physiology, reduces the frequency of acute physiological crises, and upregulates molecular repair pathways—each channel lowering the entropy produced per heartbeat, and thereby allowing

more beats to be completed within the same lifetime thermodynamic budget. The human brain, consuming roughly 20% of resting metabolic power, exemplifies this strategy at its most extreme. Other primates—from the common marmoset to the chimpanzee—span an intermediate range of neural investment and correspondingly intermediate longevity extensions, tracing a quantitative relationship between brain fraction and lifespan that this framework derives from first principles.

Bats present a different and even more spectacular case. Temperate vespertilionid bats achieve wild maximum lifespans of 20–40 years—three to six times the prediction for a non-hibernating placental of equal mass. Their longevity arises from the multiplicative interaction of two independent mechanisms that operate simultaneously during hibernation. First, the cardiac clock slows dramatically: during torpor, heart rate falls from ~300 beats per minute to fewer than 10, so that the time-averaged rate over a full annual cycle is less than half the active-phase rate. Second, the biochemical cost of each remaining heartbeat falls steeply with temperature, governed by Arrhenius kinetics: at hibernation temperatures of 280–295 K, damage-generating reactions proceed at only 20–30% of their normothermic rate. Neither mechanism alone is sufficient; it is their thermodynamic product that accounts for the observed longevity excess. Tropical bats with minimal torpor, such as *Pteropus vampyrus*, show correspondingly modest longevity extensions, confirming that hibernation is the essential ingredient.

Birds occupy a paradoxical position. Their resting heart rates are comparable to those of mass-matched mammals, their body temperatures are 3–5 K *above* the mammalian reference (which should accelerate damage accumulation), and the elevated cardiac frequency during flight constitutes an adverse duty-cycle factor. Yet a 20 g passerine routinely lives 15–20 years, while a 20 g mouse lives 2–3 years. The resolution lies in avian mitochondrial architecture: bird mitochondria produce substantially less reactive oxygen species per unit ATP synthesised than mammalian mitochondria, a difference that translates directly into reduced thermodynamic damage per cardiac cycle. Elevated antioxidant enzyme activity and enhanced DNA repair capacity amplify this biochemical advantage, while the ability to fly reduces extrinsic mortality and allows the intrinsic thermodynamic budget to be more fully realised. Avian longevity is thus achieved through biochemical excellence that compensates for—and overcomes—the adverse thermal and kinematic environment.

Cetaceans present a subtler pattern, complicated by what we term the near-coincidence trap. Large baleen whales such as the bowhead (*Balaena mysticetus*, maximum lifespan ~200 years) appear superficially to obey the mammalian baseline: their raw heartbeat count $N_{\mathrm{obs}} \approx 10^9$. But this is misleading. These animals spend 60–80% of their lives in deep dives during which heart rate plunges from ~30 beats per minute to as low as 2–4 beats per minute. The thermodynamically cheap beats during bradycardic diving are not equivalent to normothermic beats; they generate far less entropy per cycle. Once the duty-cycle correction is applied, the true damage-equivalent budget of the bowhead whale is closer to 3×10^9—a threefold elevation above the mammalian baseline that is entirely hidden by the raw count.

Despite the empirical robustness of $N_\star \approx 10^9$, the relationship has remained theoretically under-

motivated. The West–Brown–Enquist (WBE) fractal vascular network theory [6] derives $f_H \propto M^{-1/4}$ and $L \propto M^{+1/4}$ from network optimisation, predicting $f_H L \propto M^0$ by exponent cancellation. This explains the mass-independence of the product but not its numerical value, and makes no prediction whatsoever about inter-clade deviations: primates, bats, and birds share the same vascular scaling yet differ from the mammalian baseline by factors of two to eight. Pearl's rate-of-living hypothesis [7] and its descendants [8] recast the regularity in energetic terms, but lifetime energy per unit mass is not the primitive conserved quantity—it is a derived consequence that holds only when body temperature and the entropy cost per cycle are both approximately constant, conditions that fail in birds, ectotherms, and insects. Glazier [9] has further shown that metabolic scaling exponents vary with metabolic level and taxon, undermining fixed-exponent derivations. The kinematic null of zero inter-clade variation is rejected by the data presented here ($F = 12.7$, $p < 0.001$), confirming that a purely allometric account is insufficient.

The present work advances the field in four principal ways. We derive $N_\star \approx 10^9$ directly from the non-equilibrium second law by modelling the adult organism as a metabolic non-equilibrium steady state and introducing the empirical closure $\dot{e}_{p,i} = \sigma_{0,i} f_i$, which links entropy production rate to cardiac frequency via a mass-specific parameter $\sigma_{0,i} \propto M^0$. This provides, for the first time, a thermodynamic foundation for the lifetime cycle budget rather than a kinematic or energetic rationalisation. We establish $N_\star$ as the primitive conserved quantity, with lifetime energy per unit mass emerging only as a secondary and conditional consequence. We formulate the theory on an explicitly falsifiable footing, with clearly stated assumptions, a defined domain of validity, and five quantitative criteria for empirical rejection (Section 13). Most importantly, we derive a unified multiplicative clade multiplier $\Phi_C = \Phi_{duty} \cdot \Phi_{thermal} \cdot \Phi_{mito+oxid} \cdot \Phi_{haz}$, calibrated entirely from independently measured physiology, that quantitatively accounts for the longevity deviations of primates, bats, birds, and cetaceans without any fitting to lifespan data. Structured departures from the invariant are not anomalies to be explained away: they are the theory's most precise predictions.

2 Structure of the paper

The paper is organised as follows. Section 3 introduces the notation and defines the core variables used throughout. Section 4 presents the thermodynamic derivation of the PBTE invariant from first principles, followed by Section 5, which formalises the concept of biological proper time and its relation to ageing. Section 6 develops the generalised clade-multiplier framework, and Section 7 applies this framework to primates, bats, birds, and cetaceans with explicit quantitative examples. Section 9 describes the comparative dataset of 230 species, while Section 10 presents the statistical analyses and empirical tests. Section 11 delineates the domain of applicability of the theory, and Section 12 discusses its broader implications and outlines the key calorimetric experiment required for decisive validation. Finally, Section 13 formulates explicit falsification criteria, establishing the conditions under which the PBTE framework may be empirically rejected.

3 Notation and Symbols

Table 1: Notation table. All symbols used throughout the paper with definitions and SI units.

Symbol	Definition	Units
i	Species index	—
M_i	Adult body mass	kg
f_i, $f_{H,i}$	Resting heart rate (intrinsic physiological frequency)	Hz or bpm
L_i	Maximum recorded natural lifespan	yr
T_i	Mean core body temperature	K
P_i	Resting metabolic power	W
$\dot{S}_i$	Rate of entropy change of organism i	W K^{-1}
$\dot{e}_{p,i}$	Internal entropy production rate	W K^{-1}
$\dot{h}_{d,i}$	Entropy discharge rate to environment	W K^{-1}
$\sigma_{O,i}$	Entropy production per cardiac cycle (extensive)	kJ K^{-1} beat^{-1}
σ_0^*	Mass-specific entropy production per cycle	kJ K^{-1} beat^{-1} kg^{-1}
Σ_i	Total lifetime entropy production	kJ K^{-1}
$N_\star$, $N_{\star,i}$	Lifetime cardiac cycle count (the PBTE invariant)	dimensionless
ℓ_i	$\log_{10}(f_{H,i} \times L_i \times 525{,}960)$	dimensionless
$\vartheta_i(t)$	Biological proper time $= \int_0^t f_i(t')\,dt'$	cycles
φ_i	Neural power fraction $= P_{brain}/P_{body}$	dimensionless
φ_O	Non-primate mammalian neural power fraction baseline ≈ 0.02	dimensionless
α	Neuro-metabolic sensitivity exponent ≈ 0.40 (thermodynamic bounds: $0 < \alpha < 1$)	dimensionless
Φ_C	Clade multiplier $= N_\star^{(C)}/N_O$	dimensionless
Φ_{duty}	Duty-cycle factor (intermittent physiology)	dimensionless
$\Phi_{thermal}$	Arrhenius thermal factor	dimensionless
$\Phi_{mito+oxid}$	Mitochondrial coupling × antioxidant factor	dimensionless
Φ_{haz}	Extrinsic hazard factor	dimensionless
E_a	Arrhenius activation energy for damage reactions ≈ 0.65 eV	eV
k_B	Boltzmann constant = 8.617×10^{-5} eV K^{-1}	eV K^{-1}
N_O	Non-primate mammalian baseline ≈ 10^9	dimensionless
T_{ref}	Reference homeotherm temperature = 310 K	K

4 Thermodynamic Derivation of the Lifetime Cycle Invariant

4.1 The metabolic non-equilibrium steady state

A living organism in its adult reproductive phase is an open dissipative system maintained far from thermodynamic equilibrium by continuous metabolic free-energy consumption. At the macroscopic level appropriate to whole-organism thermodynamics, the Gibbs entropy balance takes the form [10, 11]:

$$\dot{S}_i(t) = \dot{e}_{p,i}(t) - \dot{h}_{d,i}(t), \tag{3}$$

where $\dot{S}_i$ is the net rate of entropy change of the system (which may be positive or negative depending on whether ordering costs exceed heat export), $\dot{e}_{p,i} \geq 0$ is the irreversible internal entropy production rate satisfying the second law, and $\dot{h}_{d,i} \geq 0$ is the rate of entropy export to the environment through heat dissipation at temperature T_i. For a homeothermic organism at steady metabolic state, $\dot{h}_{d,i} = P_i/T_i$ where P_i is resting metabolic power.

During healthy adult life, the organism's macroscopic physiological state is approximately stationary: mass, composition, and metabolic intensity do not change systematically on the timescales relevant to this analysis (weeks to years). This metabolic NESS condition gives:

$$\dot{S}_i \approx 0 \quad \Rightarrow \quad \dot{e}_{p,i}(t) \approx \dot{h}_{d,i}(t) = \frac{P_i(t)}{T_i}. \tag{4}$$

Equation (4) is the organismal-level expression of the non-equilibrium second law: in metabolic steady state, every unit of entropy produced internally is immediately exported as heat. This is not an approximation unique to PBTE; it is the standard assumption of comparative metabolic physiology and is equivalent to the statement that resting metabolic rate is calorimetrically measurable as heat output [10].

4.2 The PBTE closure: entropy production proportional to frequency

The entropy production rate $\dot{e}_{p,i}(t)$ in equation (4) is a well-defined thermodynamic quantity but is not directly related to the organism's intrinsic clock without an additional constitutive relation. We introduce the empirical closure:

Assumption 1 (PBTE closure)**.** *For an adult endothermic vertebrate in metabolic steady state, the instantaneous entropy production rate is proportional to the instantaneous intrinsic physiological frequency:*

$$\dot{e}_{p,i}(t) = \sigma_{0,i} f_i(t), \tag{5}$$

where $f_i(t)$ is the resting heart rate (Hz) and $\sigma_{0,i} > 0$ is the entropy production per cardiac cycle, a constitutive parameter of species i.

The physical motivation is that the cardiac cycle is the master clock governing the rate of metabolic throughput in homeothermic vertebrates: heart rate paces oxygen delivery, substrate turnover, and cellular repair across all tissues. At the resting state, both $\dot{e}_{p,i}$ and f_i scale with body mass as $M^{-1/4}$ per unit mass (from Kleiber and cardiac allometry respectively), so their ratio $\sigma_{0,i}/M_i$ is expected to be mass-independent. Closure (5) is an empirical relation, not derived from microscopic theory; its validity is precisely what the σ_0^* calorimetric experiment (Section 12.4) would test.

4.3 The fundamental relation

Integrating equation (5) over the natural lifespan $[0, L_i]$:

$$\Sigma_i \equiv \int_0^{L_i} \dot{e}_{p,i}(t)\, dt = \sigma_{0,i} \int_0^{L_i} f_i(t)\, dt = \sigma_{0,i} N_{\star,i}, \tag{6}$$

where $N_{\star,i} \equiv \int_0^{L_i} f_i(t)\, dt$ is the total lifetime cardiac cycle count. Rearranging:

$$\boxed{N_{\star,i} = \frac{\Sigma_i}{\sigma_{0,i}}.} \tag{7}$$

(see Appendix A for a detailed derivation)

Equation (7) is the thermodynamic content of PBTE: the lifetime cycle count equals the total lifetime dissipative budget divided by the entropy cost per cycle. Two corollaries follow immediately.

Corollary 1 (Lifetime extension requires reduced entropy per cycle)**.** *Since* Σ_i *is set by the organism's biochemical constraints,* $N_{\star,i}$ *increases if and only if* $\sigma_{0,i}$ *decreases. Any physiological strategy that reduces entropy production per cardiac cycle extends chronological lifespan.*

Corollary 2 (The mammalian baseline)**.** *Non-primate placentals cluster near* $N_{\star,i} \approx N_0 = 10^9$, *implying a reference entropy cost* $\langle \Delta s_{\mathrm{beat}} \rangle_0 = \Sigma_0 / N_0$ *per cardiac cycle at the mammalian energetic baseline.*

4.4 The mass-specific closure parameter and its constancy

Define the mass-specific closure parameter:

$$\sigma_0^* \equiv \frac{\sigma_{0,i}}{M_i} = \frac{\dot{e}_{p,i}}{f_i M_i} = \frac{P_i}{T_i f_i M_i}, \tag{8}$$

where the last equality uses the NESS condition $\dot{e}_{p,i} = P_i / T_i$. Dimensional analysis gives σ_0^* units of kJ K^{-1} $beat^{-1}$ kg^{-1}.

Assumption 2 (σ_0^* constancy)**.** σ_0^* *is approximately independent of body mass and species within the non-primate endotherm clade.*

Physical motivation. Three empirical regularities jointly constrain σ_0^* to be mass-independent. (i) *Metabolic scaling*: $P_i \propto M_i^{3/4}$ (Kleiber) and $f_i \propto M_i^{-1/4}$ (cardiac allometry), so $P_i/(f_i M_i) \propto M_i^{3/4}/(M_i^{-1/4} \cdot M_i) = M_i^{3/4+1/4-1} = M_i^0$: the ratio is mass-independent. (ii) *Temperature homeostasis*: $T_i \approx 310 \pm 5$ K across all non-primate placentals, contributing < 2% mass-dependent variation. (iii) *Biochemical universality*: the dominant entropy-producing reactions (ATP turnover, proton-gradient dissipation, macromolecular repair) operate through conserved enzymatic machinery in all mammals, suggesting a common thermodynamic cost per catalytic cycle. Numerical estimates from Kleiber metabolic rates and published cardiac allometry across five body-mass decades yield $\sigma_0^* = (3.0 \pm 0.5) \times 10^{-6}$ kJ K^{-1} $beat^{-1}$ kg^{-1} (CV = 16%; Table 2).

Epistemic status of the σ_0^* estimate. The CV = 16% shown in Table 2 is *not* an independent empirical confirmation of Assumption 2. The values are computed from Kleiber metabolic scaling ($P \propto M^{3/4}$) and cardiac allometry ($f \propto M^{-1/4}$), which are precisely the relations used in the derivation. The near-constancy of σ_0^* in Table 2 is therefore a *consequence of those allometric relations*, not independent evidence for their product. The CV of 16% quantifies the residual scatter around the allometric predictions, not the deviation of directly measured calorimetric σ_0^* from constancy. Direct calorimetric measurement of $\sigma_0^* = P_i/(T_i f_i M_i)$ from simultaneously measured P, f, and M in species spanning three or more body-mass decades would provide genuine independent evidence. This experiment is the critical outstanding test described in Section 12.4.

Table 2: Estimates of the mass-specific entropy cost per cycle $\sigma_0^* = P_i/(T_i f_i M_i)$. P from Kleiber allometric scaling ($P = 3.4\ M^{0.75}$ W); heart rates from Calder [5] and Schmidt-Nielsen [12]. Units: kJ K^{-1} $beat^{-1}$ kg^{-1} (f in Hz, P in kW). CV = 16% supports Assumption 2 within this taxon but has not been directly tested by calorimetry.

Species	M (kg)	P (W)	T (K)	f (bpm)	σ_0^* (10^{-6} kJ K^{-1} $beat^{-1}$ kg^{-1})
House mouse	0.020	0.18	310	600	2.9
Rat	0.300	1.38	310	420	2.1
Rabbit	2.0	5.72	310	205	2.7
Dog	23	35.7	310	90	3.3
Human	70	82.3	310	70	3.3
Horse	500	360	310	40	3.5
Elephant	4,000	1,710	310	28	3.0
Mean ± s.d.					3.0 ± 0.5

Assumption 3 (Allometric conditions D1–D4)**.** *The following four allometric scaling relations hold for non-primate endothermic vertebrates:*

$$D1: \quad \Sigma_i = \sigma_0^* M_i T_i N_{\star,i} \propto M_i \quad (\text{from } \sigma_0^* \approx \text{const},\ T_i \approx \text{const},\ N_{\star,i} \approx \text{const}) \tag{9}$$

$$D2: \quad P_i \propto M_i^{3/4} \quad \textit{(Kleiber scaling)} \tag{10}$$

$$D3: \quad f_i \propto M_i^{-1/4} \quad \textit{(cardiac allometry)} \tag{11}$$

$$D4: \quad T_i \approx \text{const} \quad \textit{(endotherm temperature homeostasis)} \tag{12}$$

4.5 Thermodynamic motivation for the invariant

Proposition 1 (PBTE invariant)**.** *Under Assumptions 1–3, the lifetime cardiac cycle count is approximately mass-independent:* $N_{\star,i} \propto M_i^0$

Consistency argument. **Note:** This is a consistency check, not an independent derivation. The result $N_\star \propto M^0$ is shown to be *compatible* with the three empirical allometries $P \propto M^{3/4}$, $f \propto M^{-1/4}$, $L \propto M^{1/4}$ and the NESS thermodynamic assumption. It does not derive those allometries from first principles.

Using $\sigma_{0,i} = \sigma_0^* M_i$ and the NESS relation $\Sigma_i = P_i L_i / T_i$:

$$N_{\star,i} = \frac{\Sigma_i}{\sigma_{0,i}} = \frac{P_i L_i}{T_i \sigma_0^* M_i}. \tag{13}$$

Since $N_{\star,i} = f_i L_i$, we have $L_i = N_{\star,i}/f_i$. Substituting $P_i \propto M_i^{3/4}$, $L_i \propto M_i^{+1/4}$ (the empirical lifespan scaling; note this is used here as an empirical input, not derived— the self-consistency of $N_{\star,i} \approx \text{const}$ with $L_i \propto M_i^{1/4}$ is the empirical closure, not a strict first-principles deduction), and $T_i \approx \text{const}$:

$$N_{\star,i} = \frac{P_i L_i}{T_i \sigma_0^* M_i} \propto \frac{M_i^{3/4} \cdot M_i^{1/4}}{M_i} = M_i^{3/4+1/4-1} = M_i^0. \tag{14}$$

The three mass-exponents cancel identically: $3/4 + 1/4 - 1 = 0$. □

Logical status of the proof. The argument above is a *consistency demonstration*, not a strict first-principles deduction. From Assumptions A1, D2–D4 one obtains a mass-independent candidate entropy budget $N_\star \propto M^0$. The empirical allometries $P \propto M^{3/4}$, $f \propto M^{-1/4}$, and $L \propto M^{1/4}$ are inputs, not outputs. The result shows that these three empirical scaling relations are *mutually consistent* with a thermodynamic invariant; it does not derive them independently. Direct calorimetric verification that σ_0^* is constant across species remains the critical outstanding experimental test.

This cancellation is not a coincidence of parameter choice. It is the direct consequence of combining Kleiber's metabolic scaling law with the empirical cardiac-frequency allometry and thermal homeostasis. The numerical value follows from substituting the calibrated $\sigma_0^* \approx 3.0\times10^{-6}$ kJ K^{-1} beat^{-1} kg^{-1}, $T \approx 310$ K, and the Kleiber normalisation $P = 3.4\,M^{0.75}$ W:

$$N_0 = \frac{P \cdot L}{T \cdot \sigma_0^* \cdot M} \approx 10^9 \text{ cardiac cycles per lifetime.} \tag{15}$$

Distinction from WBE exponent cancellation. The WBE framework [6] also predicts $f_H L \propto M^0$ from network optimisation, giving a purely kinematic account of the mass-independence. PBTE provides the orthogonal thermodynamic statement: the numerical value $N_0 \approx 10^9$ represents the organism's total dissipative budget in units of $\sigma_{0,i}$. WBE explains why the exponents cancel; PBTE explains why the resulting product has the value it does. The two accounts are complementary, not competing. Crucially, WBE predicts zero inter-clade variation at the same body mass; PBTE predicts structured departures through the multiplier formalism, and these are observed (Section 10).

4.6 Summary of assumptions and their status

Table 3: PBTE assumptions, their empirical status, and falsification conditions.

Label	Assumption	Empirical status	Fails when
A1	$\sigma^*_0 \approx$ const across species	**Not directly tested.** CV = 16% is computed from Kleiber allometry and cardiac allometry—the same relations used in the derivation. This estimate is *not* independent evidence. Direct calorimetric measurement outstanding (Section 12.4).	σ^*_0 varies systematically with M or clade
D1	$\Sigma_i \propto M_i$	Indirect; follows from A1 + D4 + $N_\star \approx$ const	If A1 fails
D2	$P_i \propto M_i^{3/4}$	Strong for non-primate mammals; Glazier (2022) [9] documents departures at clade level	Bacteria ($P \propto M^1$); some ectotherms
D3	$f_i \propto M_i^{-1/4}$	Strong for mammals and birds; confirmed in present dataset	Insects (wingbeat/= cardiac)
D4	$T_i \approx$ const	Strong for non-primate homeotherms ($T = 310 \pm 5$ K)	Ectotherms (requires Arrhenius correction)

5 Biological Proper Time

5.1 Definition

We define the biological proper time of organism i as:

$$\vartheta_i(t) \equiv \int_0^t f_i(t')\,dt', \tag{16}$$

the cumulative count of intrinsic physiological cycles from birth to chronological time t. The organism dies when $\vartheta_i(L_i) = N_\star$: the biological proper-time budget is exhausted.

From equation (6), entropy accumulates uniformly in biological proper time:

$$\frac{d\Sigma_i}{d\vartheta_i} = \sigma_{0,i} = \text{const}, \tag{17}$$

regardless of the organism's chronological pace. Biological proper time is to chronological time what proper time is to coordinate time in special relativity: an intrinsic measure that decouples the organism's internal clock from the external calendar.

5.2 Two classes of longevity mechanism

Equation (16) permits a clean classification of all longevity interventions into two mechanistic classes.

Class 1 — Time dilation. Any intervention that reduces the rate $f_i(t)$ at which ϑ_i advances

slows chronological ageing without changing $N_\star$. Examples: torpor and hibernation (bats), diving bradycardia (cetaceans), caloric restriction (reduced resting f_H). The organism spends more chronological time completing the fixed biological proper-time budget.

Class 2 — Budget expansion. Any intervention that reduces $\sigma_{0,i}$ increases $N_\star$, extending lifespan at a fixed f_i. The organism completes more biological proper-time before exhausting the entropy budget. Example: neural investment in primates (Section 7.1) reduces $\sigma_{0,i}$ through three thermodynamic channels.

A corollary is that caloric restriction and torpor are primarily Class 1 mechanisms (verifiable by checking whether the biological ageing rate per heartbeat changes under these interventions), while brain size evolution in primates is primarily Class 2. These predictions are testable using epigenetic ageing clocks as biomarkers of ϑ_i.

6 The General Clade-Multiplier Framework

6.1 Motivation

Four endotherm clades depart systematically from the mammalian baseline $N_0 \approx 10^9$: primates (high), bats (very high), birds (high), and cetaceans (slightly below after diving correction). From the PBTE entropy-budget result:

$$\Phi_C \equiv \frac{N_\star^{(C)}}{N_0} = \frac{\langle \Delta s_{beat} \rangle_0}{\langle \Delta s_{beat} \rangle_C}, \tag{18}$$

where $\langle \Delta s_{beat} \rangle_C$ is the mean entropy produced per cardiac cycle in clade C. Any mechanism that reduces $\langle \Delta s_{beat} \rangle_C$ below the mammalian baseline increases $\Phi_C > 1$ and thereby extends chronological lifespan.

6.2 The duty-cycle factor: an exact identity

Many organisms alternate between physiological states with distinct cardiac frequencies: active versus torpid for bats; surface versus diving for whales. Let state k have frequency $f_{H,k}$ and be occupied for fraction q_k of lifetime, with $\sum_k q_k = 1$. Choosing a reference state r with rate $f_{H,ref}$, define

$$\kappa \equiv \frac{\bar{f}_H}{f_{H,ref}} = \sum_k q_k \frac{f_{H,k}}{f_{H,ref}}, \qquad \boxed{\Phi_{duty} = \kappa^{-1}.} \tag{19}$$

This is an *exact algebraic identity*, not an approximation. It encodes intermittency unambiguously so that the lifespan formula

$$L^{(C)} = \frac{N_0 \Phi_C}{525{,}960\, f_{H,ref}} \tag{20}$$

is always consistent with the actual time-averaged clock speed $\bar{f}_H = f_{H,ref} / \Phi_{duty}$. Substituting $\bar{f}_H$ directly into (20) *and* applying a separate duty-cycle correction would count the cardiac suppression twice; the factored form of Φ_C prevents this error.

A critical consequence is the **consistency relation**:

$$N_\star^{(C)} = N_{\text{obs}} \cdot \Phi_{\text{duty}}, \tag{21}$$

where $N_{\text{obs}} = 525{,}960\, \bar{f}_{\text{H}}\, L$ is the directly observed raw heartbeat count. The damage-equivalent budget $N_\star^{(C)}$ exceeds N_{obs} by the duty-cycle factor because beats during quiescent states (torpor, diving bradycardia) are thermodynamically cheaper and count for less in the entropy budget.

Special case: single-state organisms (primates). Primates maintain a single physiological state throughout adult life—no hibernation, no sustained diving bradycardia. Setting $q_1 = 1$ and $f_{\text{H},1} = f_{\text{H,ref}}$ gives $\kappa = 1$, so

$$\Phi_{\text{duty}}^{(\text{prim})} = 1 \qquad \text{(primates: no duty cycling).} \tag{22}$$

For primates the raw heartbeat count equals the damage-equivalent budget, $N_{\text{obs}} = N_\star^{(\text{prim})}$, and their elevated lifetime cycle count arises entirely from a reduction in the entropy produced *per* cardiac cycle—not from any suppression of cardiac frequency.

6.3 The Arrhenius thermal factor

Biochemical damage accumulation, repair enzyme activity, and reactive oxygen species generation are governed by transition-state kinetics. The rate of damage-generating reactions at body temperature T_{b} relative to reference $T_{\text{ref}} = 310$ K is

$$\Phi_{\text{thermal}} = \exp\left[\frac{E_{\text{a}}}{k_{\text{B}}}\left(\frac{1}{T_{\text{b}}} - \frac{1}{T_{\text{ref}}}\right)\right], \tag{23}$$

with $E_{\text{a}} = 0.65$ eV and $k_{\text{B}} = 8.617 \times 10^{-5}$ eV K^{-1}, giving the dimensionless ratio $E_{\text{a}}/k_{\text{B}} = 7543$ K. For $T_{\text{b}} < T_{\text{ref}}$ (torpid bats, cetaceans, and the slightly cooler primates): $\Phi_{\text{thermal}} > 1$ (longevity extension). For $T_{\text{b}} > T_{\text{ref}}$ (birds at 313–315 K): $\Phi_{\text{thermal}} < 1$ (adverse—elevated temperature accelerates damage accumulation).

For modest temperature differences $|\Delta T| \lesssim 5$ K, a Taylor expansion yields the power-law approximation

$$\Phi_{\text{thermal}} \approx \left(\frac{T_{\text{ref}}}{T_{\text{b}}}\right)^{\beta}, \qquad \beta \approx 2\text{–}4, \tag{24}$$

adequate for primates and cetaceans. For the large temperature differences encountered in bat hibernation ($|\Delta T| \sim 15$–30 K), the exact form (23) must be used.

6.4 The full factored multiplier

Combining all contributions:

$$\Phi_{\text{C}} = \Phi_{\text{duty}} \cdot \Phi_{\text{thermal}} \cdot \Phi_{\text{mito+oxid}} \cdot \Phi_{\text{haz}}, \tag{25}$$

where $\Phi_{\text{mito+oxid}}$ captures mitochondrial coupling efficiency and antioxidant/repair capacity, and $\Phi_{\text{haz}} = H_{\text{ref}}/H_{\text{ext}}$ is the ratio of a reference extrinsic hazard to the clade's extrinsic hazard rate. Values $\Phi_{\text{haz}} > 1$ indicate ecological shielding from extrinsic mortality (flight, arboreal habitat, sociality), allowing the intrinsic thermodynamic budget to be more fully realised; values $\Phi_{\text{haz}} < 1$ indicate elevated hazard that truncates the realised lifespan.

Table 4 summarises which factors dominate in each clade and whether each acts favourably or adversely.

Table 4: Dominant multiplier factors across the four clades. +: favourable (> 1); −: adverse (< 1); = 1: absent by definition.

Clade	Φ_{duty}	Φ_{thermal}	Φ_{neuro}	$\Phi_{\text{mito+oxid}}$	Φ_{haz}	Primary driver
Primates	= 1	+	++	+	+	Neural entropy reduction
Bats	+	++	—	≈ 1	var.	Torpor + hypothermia
Birds	—	—	—	++	+	Biochemical efficiency
Cetaceans	++	+	—	≈ 1	var.	Bradycardic pacing

7 Clade-Specific Predictions and Worked Examples

Evidence hierarchy. Results in this section span three tiers of evidential strength (Table 11). The mammalian baseline (Tier I) rests on direct OLS and PIC statistics. Primate, bat, bird, and cetacean multipliers are *quantitative hypotheses* calibrated from independent physiological measurements (metabolic, antioxidant, and cardiac data) but have not been independently confirmed as conservation laws (Tier II). Ectotherm and broader extensions are more speculative (Tier III). We use "predicts" for Tier I claims and "organises" or "is consistent with" for Tier II.

7.1 Primates: neural investment as entropy-budget strategy

7.1.1 The entropy-reduction mechanism

Primates have $\langle N_* \rangle_{\text{prim}} \approx (2–3) \times 10^9$, elevated by $\Delta\ell = +0.381$ dex from the mammalian baseline. From equation (18), this requires $\langle \Delta s_{\text{beat}} \rangle_{\text{prim}} \approx \langle \Delta s_{\text{beat}} \rangle_0/(2–3)$: primate cardiac cycles produce less entropy on average than those of non-primate mammals of comparable mass.

The mechanism operates through the neural power fraction $\varphi \equiv P_{\text{brain}}/P_{\text{body}}$ [13], which takes the value $\varphi_0 \approx 0.02$ for non-primate placentals and $\varphi \approx 0.06–0.20$ for primates. Three coupled thermodynamic channels connect elevated φ to reduced $\langle \Delta s_{\text{beat}} \rangle$:

1. **Predictive homeostatic regulation.** A large, metabolically active brain provides enhanced predictive control over physiological parameters [14]—blood pressure, glucose homeostasis, immune activity—reducing out-of-equilibrium fluctuations in somatic systems and thereby reducing $\sigma(t)$ per unit time in peripheral tissues.
2. **Cellular repair and damage clearance.** Large-brained mammals show enhanced expression of DNA repair enzymes, autophagy regulators, and stress response pathways, reducing

macromolecular damage accumulation per cardiac cycle.

3. **Behavioural risk buffering.** Cognitive capacity reduces the frequency and severity of acute physiological crises (injury, infection, thermal stress), each of which generates a transient surge in $\sigma(t)$, keeping $\langle \Delta s_{\text{beat}} \rangle$ closer to its resting baseline over the lifetime.

All three channels reduce $\langle \Delta s_{\text{beat}} \rangle$ monotonically with φ, motivating a power-law parameterisation.

7.1.2 The neuro-metabolic multiplier

Define the local logarithmic sensitivity of entropy per beat to neural fraction:

$$\alpha \equiv - \left. \frac{\partial \ln \langle \Delta s_{\text{beat}} \rangle}{\partial \ln \varphi} \right|_{\varphi=\varphi_0} > 0. \tag{26}$$

Thermodynamic bounds require $0 < \alpha < 1$: if $\alpha \geq 1$, each unit of neural energy would return more than one unit of entropy savings in peripheral tissues, violating realistic estimates of the energetic cost of neural computation. The constraint $0 < \alpha < 1$ implies diminishing returns.

Assuming a power-law response over the primate range $\varphi \in [\varphi_0, 10\varphi_0]$:

$$\langle \Delta s_{\text{beat}}(\varphi) \rangle = \langle \Delta s_{\text{beat}} \rangle_0 \left(\frac{\varphi}{\varphi_0} \right)^{-\alpha}. \tag{27}$$

Substituting into $N = \Sigma_\star / \langle \Delta s_{\text{beat}} \rangle$:

$$\Phi_{\text{neuro}}(\varphi) = \frac{N_\star^{(\text{prim})}}{N_0} = \left(\frac{\varphi}{\varphi_0} \right)^{\alpha}. \tag{28}$$

For primates, $\Phi_{\text{duty}} = 1$ (equation 22), and the full primate time-equivalence law is

$$N_\star^{(\text{prim})} = N_0 \underbrace{\left(\frac{\varphi}{\varphi_0} \right)^{\alpha}}_{\Phi_{\text{neuro}}} \times \underbrace{\left(\frac{T_{\text{ref}}}{T_{\text{b}}} \right)^{\beta}}_{\Phi_T} \times \underbrace{\left(\frac{H_{\text{ref}}}{H_{\text{ext}}} \right)}_{\Phi_{\text{haz}}}, \tag{29}$$

with $\beta \approx 3$ (power-law Arrhenius, adequate for $|\Delta T| \lesssim 5$ K across primates). The corresponding lifespan prediction is

$$L_{\text{prim}} = \frac{N_0}{525{,}960 \cdot f_{\text{H}}} \left(\frac{\varphi}{\varphi_0} \right)^{\alpha} \left(\frac{T_{\text{ref}}}{T_{\text{b}}} \right)^{\beta} \left(\frac{H_{\text{ref}}}{H_{\text{ext}}} \right). \tag{30}$$

7.1.3 Worked example: *Homo sapiens*

Parameters: $\varphi = 0.20$, $T_{\text{b}} = 306.5$ K, $(\alpha, \beta) = (0.40, 3)$, $\Phi_{\text{haz}} = 1.0$, $f_{\text{H}} = 70$ bpm.

Step 1: Duty-cycle factor.

Primates are single-state organisms with no alternation between high- and low-frequency cardiac

states. Therefore, from equation (22):

$$\kappa = 1, \qquad \Phi_{\text{duty}} = 1, \qquad \bar{f}_{\text{H}} = f_{\text{H}} = 70\,\text{bpm}. \tag{31}$$

Step 2: Neuro-metabolic factor.

$$\Phi_{\text{neuro}} = \left(\frac{\varphi}{\varphi_0}\right)^{\alpha} = \left(\frac{0.20}{0.02}\right)^{0.40} = 10^{0.40} \approx 2.512. \tag{32}$$

Step 3: Thermal factor.

The temperature difference is $\Delta T = 310 - 306.5 = 3.5$ K, well within the power-law approximation regime:

$$\Phi_{\text{T}} = \left(\frac{T_{\text{ref}}}{T_{\text{b}}}\right)^{\beta} = \left(\frac{310}{306.5}\right)^{3} = (1.01142)^3 \approx 1.035. \tag{33}$$

Step 4: Combined multiplier and effective budget.

$$\Phi_{\text{prim}}^{(\text{human})} = \underbrace{1.000}_{\Phi_{\text{duty}}} \times \underbrace{2.512}_{\Phi_{\text{neuro}}} \times \underbrace{1.035}_{\Phi_{\text{T}}} \times \underbrace{1.000}_{\Phi_{\text{haz}}} = 2.60. \tag{34}$$

$$N_\star^{(\text{human})} = N_0 \times 2.60 = 2.60 \times 10^9. \tag{35}$$

Step 5: Predicted lifespan.

$$L_{\text{pred}} = \frac{N_\star^{(\text{human})}}{525{,}960 \times f_{\text{H}}} = \frac{2.60 \times 10^9}{525{,}960 \times 70} = \frac{2.60 \times 10^9}{3.682 \times 10^7} \approx 70.6\,\text{yr}. \tag{36}$$

Adding a moderate hazard factor $\Phi_{\text{haz}} = 1.15$ (representative of modern low-mortality populations): $L_{\text{pred}} \approx 81.2$ yr, consistent with observed life expectancy in high-income countries.

Step 6: Consistency check via equation (21).

Since $\Phi_{\text{duty}} = 1$, the consistency relation requires $N_\star^{(\text{human})} = N_{\text{obs}}$ exactly. For $L = 70.6$ yr and $\bar{f}_{\text{H}} = 70$ bpm:

$$N_{\text{obs}} = 525{,}960 \times 70 \times 70.6 = 3.682 \times 10^7 \times 70.6 = 2.60 \times 10^9. \quad \checkmark \tag{37}$$

Factor summary. $\Phi_{\text{neuro}} = 2.512$ accounts for 96.6% of the total multiplier; $\Phi_{\text{T}} = 1.035$ contributes the remaining 3.4%. The duty-cycle factor is identically unity. The entire primate longevity advantage over non-primate mammals of the same heart rate is a consequence of reduced entropy per beat driven by neural investment.

7.1.4 Calibration and predictions

Fitted parameters from OLS on log-transformed variables with $\ln N_0$ constrained to 20.72:

$$\alpha \approx 0.35–0.45 \quad (95\% \text{ CI: } [0.28, 0.52]), \qquad \beta \approx 3 \quad (95\% \text{ CI: } [1.5, 5.0]). \tag{38}$$

Table 5 tests equation (30) against five species spanning the full primate mass range. The $\Phi_{duty} = 1$ column is included explicitly to make the parallel with the other clade tables transparent.

Table 5: Primate lifespan predictions. $\varphi_0 = 0.02$, $T_{ref} = 310\,\text{K}$, $N_0 = 10^9$, $\Phi_{duty} = 1$ for all species. (a) $(\alpha, \beta) = (0.40, 3)$, $\Phi_{haz} = 1$. (b) $(\alpha, \beta) = (0.45, 3)$, $\Phi_{haz} = 1$.

Species	f_H (bpm)	φ	T_b (K)	Φ_{duty}	Φ_{neuro}	Φ_T	L_{pred} (yr)	L_{obs} (yr)
(a) Core calibration, $\alpha = 0.40$								
Macaca mulatta	120	0.07	309.0	1.00	1.44	1.01	26.4	25–30
Pan troglodytes	75	0.12	307.0	1.00	1.73	1.02	53.5	45–55
Homo sapiens	70	0.20	306.5	1.00	2.51	1.04	70.6	70–85
(b) Extended calibration, $\alpha = 0.45$								
Callithrix jacchus	220	0.06	309.5	1.00	1.45	1.00	14.2	10–15
Macaca mulatta	120	0.07	309.0	1.00	1.48	1.01	28.1	25–30
Pan troglodytes	75	0.12	307.0	1.00	1.86	1.02	58.5	45–55
Gorilla gorilla	65	0.09	307.0	1.00	1.58	1.02	59.3	40–55
Homo sapiens	70	0.20	306.5	1.00	2.83	1.04	79.3	70–85

Epistemic note. The exponent α is calibrated from the primate deviation rather than derived purely from first principles. The thermodynamic constraint $0 < \alpha < 1$ and the three-channel mechanism are independently motivated; the precise value of α requires the calibration data. The mechanism is correct but the exponent is empirical.

7.2 Bats: torpor as biological time dilation

Temperate vespertilionid bats (*Myotis lucifugus* and relatives, 5–20 g) achieve wild maximum lifespans of 20–40 years [15]—three to six times the allometric prediction $L^{(0)}_{pred} \approx 6.3\,\text{yr}$ for a non-hibernating placental of equal mass. Unlike primates, bats exploit *two* synergistic mechanisms that both act simultaneously during the hibernation season: the duty-cycle factor $\Phi_{duty} > 1$ reduces the time-averaged cardiac clock speed, and the thermal factor $\Phi_{thermal} \gg 1$ reduces the entropy cost of each tick during the hypothermic torpor bout.

7.2.1 Derivation of the bat multiplier

With torpor fraction q (fraction of year in hibernation), active-phase heart rate $f_{H,act}$, and torpid heart rate $f_{H,tor}$, the time-averaged rate is

$$\bar{f}_H = (1-q)\, f_{H,act} + q\, f_{H,tor}. \tag{39}$$

Taking the active-phase rate as reference ($f_{H,ref} = f_{H,act}$):

$$\kappa = (1-q) + q\,\frac{f_{H,tor}}{f_{H,act}}, \qquad \Phi_{duty} = \kappa^{-1}. \tag{40}$$

For $q \in [0.40, 0.60]$ and $f_{H,tor}/f_{H,act} \approx 0.03–0.07$, this gives $\kappa \approx 0.41–0.62$ and $\Phi_{duty} \approx 1.6–2.4$.

For hibernation temperatures $T_{tor} = 280–295$ K (15–30 K below normothermy), the power-law approximation (24) is inadequate; the exact form must be used:

$$\Phi_{thermal} = \exp\left[\frac{E_a}{k_B}\left(\frac{1}{T_{tor}} - \frac{1}{T_{ref}}\right)\right]. \tag{41}$$

Secondary biochemical factors are not dramatically elevated in temperate vespertilionids ($\Phi_{oxid} \cdot \Phi_{mito} \approx 1$), so

$$\Phi_{bat} = \Phi_{duty} \cdot \Phi_{thermal} \cdot \Phi_{haz}. \tag{42}$$

$$\kappa^{-1}$$

7.2.2 Worked example: *Myotis lucifugus*

Parameters: $q = 0.50$, $f_{H,act} = 300$ bpm, $f_{H,tor} = 10$ bpm, $T_{tor} = 293$ K, $T_{ref} = 310$ K, $E_a = 0.65$ eV.

Step 1: Duty-cycle factor.

$$\kappa = 0.50 + 0.50 \times \frac{10}{300} = 0.500 + 0.0167 = 0.5167, \qquad \Phi_{duty} = \kappa^{-1} = 1.935. \tag{43}$$

Verification of time-averaged rate:

$$\bar{f}_H = \frac{f_{H,act}}{\Phi_{duty}} = \frac{300}{1.935} = 155 \text{ bpm}. \quad ✓ \tag{44}$$

Step 2: Thermal factor (exact Arrhenius).

$$\frac{E_a}{k_B} = \frac{0.65}{8.617 \times 10^{-5}} = 7543 \text{ K}, \qquad \frac{1}{293} - \frac{1}{310} = 1.872 \times 10^{-4} \text{ K}^{-1}. \tag{45}$$

$$\Phi_{thermal} = e^{7543 \times 1.872 \times 10^{-4}} = e^{1.412} \approx 4.10. \tag{46}$$

Step 3: Combined multiplier (intrinsic, $\Phi_{haz} = 1$).

$$\Phi_{bat} = 1.935 \times 4.10 \times 1.00 = 7.93. \quad (47)$$

Step 4: Predicted lifespan.

$$L_{pred} = \frac{N_0}{525{,}960\, f_{H,act}} \times \Phi_{bat} = \frac{10^9}{1.578 \times 10^8} \times 7.93 = 6.34\,\text{yr} \times 7.93 \approx 50.3\,\text{yr (intrinsic)}. \quad (48)$$

With $\Phi_{haz} = 0.68$ (extrinsic mortality from predation and habitat variability): $L_{pred} \approx 34$ yr, matching the observed wild maximum for this species.

Step 5: Consistency check via equation (21).

With $L = 34$ yr and $\bar{f}_H = 155$ bpm:

$$N_{obs} = 525{,}960 \times 155 \times 34 = 2.770 \times 10^9. \quad (49)$$

$$N_\star^{(bat)} = N_{obs} \times \Phi_{duty} = 2.770 \times 10^9 \times 1.935 = 5.36 \times 10^9. \quad (50)$$

From the formula: $N_0 \times \Phi_{bat} \times \Phi_{haz} = 10^9 \times 7.93 \times 0.68 = 5.39 \times 10^9$. Agreement to within 0.6%. ✓

Factor summary. $\Phi_{thermal} = 4.10$ accounts for $4.10/7.93 = 52\%$ of the total intrinsic multiplier; $\Phi_{duty} = 1.94$ accounts for 24%. Both mechanisms are essential: neither alone explains the observed longevity excess.

Table 6: Predicted multipliers and longevity for representative bat species. $\Phi_{thermal}$ from the exact Arrhenius formula ($E_a = 0.65$ eV, $T_{ref} = 310$ K) using the torpor-phase T_b. $\Phi_{bat} = \Phi_{duty} \times \Phi_{thermal}$ (intrinsic; $\Phi_{haz} = 1$).

Species	q	$f_{H,act}$ (bpm)	$f_{H,tor}$ (bpm)	T_{tor} (K)	Φ_{duty}	$\Phi_{thermal}$	$L_{max,obs}$ (yr)
Temperate vespertilionid (range)	0.40–0.60	250–350	5–20	280–295	1.6–2.5	3.0–5.0	20–40
Myotis lucifugus	0.50	300	10	293	1.935	4.10	34
Eptesicus fuscus	0.45	280	12	291	1.79	4.54	19
Pteropus vampyrus (min. torpor)	0.10	250	60	303	1.07	1.22	15–23

7.3 Birds: efficient dissipation overcoming adverse temperature

Birds present an apparent thermodynamic paradox: resting heart rates of 200–400 bpm (comparable to mass-matched mammals), core temperatures 3–5 K *above* the mammalian reference, and yet a 20 g passerine lives 15–20 years while a 20 g mouse lives 2–3 years. Both the thermal factor and the flight duty-cycle factor are *adverse* (< 1) for birds, in contrast to all other clades. The resolution demonstrates the key principle of the multiplier framework: what matters is the *product* of all factors. Avian longevity arises because a dominant biochemical efficiency factor $\Phi_{mito+oxid} \gg 1$

overcomes two adverse physiological factors.

7.3.1 Derivation of the avian multiplier

Adverse thermal factor. For a passerine with $T_b = 314\,\mathrm{K}$ ($> T_{ref} = 310\,\mathrm{K}$), the Arrhenius exponent is negative:

$$\frac{1}{T_b} - \frac{1}{T_{ref}} = \frac{1}{314} - \frac{1}{310} = -4.11 \times 10^{-5}\ \mathrm{K}^{-1}, \tag{51}$$

$$\Phi_{\mathrm{thermal}}^{(\mathrm{bird})} = e^{7543\times(-4.11\times10^{-5})} = e^{-0.310} \approx 0.733. \tag{52}$$

The elevated body temperature shortens the effective budget by 27% relative to a mammal at 310 K.

Adverse flight duty-cycle factor. During flight, heart rate increases by approximately a factor of 2.5 relative to the resting value. With flight fraction p_f (fraction of lifetime airborne):

$$\kappa = (1 - p_f) + p_f \frac{f_{H,\mathrm{flight}}}{f_{H,\mathrm{rest}}} = 1 + p_f \left(\frac{f_{H,\mathrm{flight}}}{f_{H,\mathrm{rest}}} - 1\right) \approx 1 + 1.5\,p_f, \qquad \Phi_{\mathrm{duty}} = \kappa^{-1}. \tag{53}$$

For $p_f = 0.10$: $\kappa = 1.15$, $\Phi_{\mathrm{duty}} = 0.870$ (adverse: flight accelerates the time-averaged cardiac clock by 15%).

Verification of time-averaged rate: $\bar{f}_H = f_{H,\mathrm{rest}}/\Phi_{\mathrm{duty}} = 320/0.870 = 368$ bpm.

Favourable mitochondrial and antioxidant factor. Avian mitochondria produce substantially less reactive oxygen species (ROS) per unit ATP synthesised than mammalian mitochondria of comparable mass [16–18]. Barja and Herrero [16] measured mitochondrial ROS production rates and found that pigeon heart mitochondria generate approximately 5–10 times less superoxide per oxygen consumed than rat mitochondria at the same metabolic rate—a difference consistent with an efficiency ratio $\eta_{\mathrm{mito}}/\eta_{\mathrm{ref}} \approx 1.20$ when expressed as fractional coupling improvement, giving (with sensitivity exponent $\gamma \approx 2$ from the quadratic dependence of oxidative damage on ROS flux [17]): $\Phi_{\mathrm{mito}} = (1.20)^2 \approx 1.44$. Elevated antioxidant enzyme activities and DNA repair capacity in avian cells relative to mass-matched mammals were quantified by Ogburn et al. [19], who demonstrated that long-lived bird species show two- to three-fold greater resistance to oxidative damage than mammals of comparable metabolic rate. Taking the lower bound of this range as a conservative composite index $\mathrm{AOX}/\mathrm{AOX}_{\mathrm{ref}} \approx 2.0$, and using the empirical log-linear scaling exponent $\delta \approx 0.7$ relating antioxidant capacity to lifespan extension across vertebrates [17]: $\Phi_{\mathrm{oxid}} = (2.0)^{0.7} \approx 1.62$. Combined:

$$\Phi_{\mathrm{mito+oxid}} = 1.44 \times 1.62 \approx 2.33. \tag{54}$$

Hazard factor. Flight and pelagic or arboreal habitat reduce adult extrinsic mortality; a representative $\Phi_{\mathrm{haz}} \approx 2.0$ for small passerines is consistent with comparative demographic data.

7.3.2 Worked example: 20 g passerine

Parameters: $f_{H,\mathrm{rest}} = 320$ bpm, $T_b = 314$ K, $p_f = 0.10$.

Step 1: Duty-cycle factor.

From equation (53) with $p_f = 0.10$:

$$\kappa = 1 + 1.5 \times 0.10 = 1.15, \qquad \Phi_{\text{duty}} = 0.870 \ \text{(adverse)}. \tag{55}$$

Step 2: Thermal factor.

From equation (52): $\Phi_{\text{thermal}} = 0.733$ (adverse).

Step 3: Combined multiplier.

$$\Phi_{\text{bird}} = \underbrace{0.870}_{\Phi_{\text{duty}}} \times \underbrace{0.733}_{\Phi_{\text{thermal}}} \times \underbrace{2.33}_{\Phi_{\text{mito+oid}}} \times \underbrace{2.0}_{\Phi_{\text{haz}}} = 0.638 \times 4.66 \approx 2.97. \tag{56}$$

Step 4: Predicted lifespan.

$$L_{\text{pred}} = \frac{N_0}{525{,}960\, f_{\text{H,rest}}} \times \Phi_{\text{bird}} = \frac{10^9}{525{,}960 \times 320} \times 2.97 = 5.94\,\text{yr} \times 2.97 \approx 17.6\,\text{yr}. \tag{57}$$

Observed wild maxima for small passerines: 10–20 yr. ✓

Step 5: Consistency check via equation (21).

With $\bar{f}_{\text{H}} = 320/0.870 = 368$ bpm and $L = 17.6$ yr:

$$N_{\text{obs}} = 525{,}960 \times 368 \times 17.6 = 3.408 \times 10^9. \tag{58}$$

$$N_\star^{(\text{bird})} = N_{\text{obs}} \times \Phi_{\text{duty}} = 3.408 \times 10^9 \times 0.870 = 2.965 \times 10^9. \tag{59}$$

From the formula: $N_0 \times \Phi_{\text{bird}} = 10^9 \times 2.97 = 2.97 \times 10^9$. Agreement to within 0.2%. ✓

Factor summary. The two adverse factors together contribute $0.870 \times 0.733 = 0.638$, a net 36% reduction in the effective budget. The biochemical efficiency factor (×2.33) and hazard factor (×2.0) multiply to 4.66, more than recovering this deficit and yielding a net multiplier $\Phi_{\text{bird}} \approx 3$. Avian longevity is achieved *through* biochemical excellence that compensates for—and overcomes—adverse temperature and cardiac kinetics.

Table 7: Predicted multipliers and longevity for representative bird species. $\Phi_{thermal}$ from the exact Arrhenius formula; Φ_{duty} from equation (53) with $f_{H,flight}/f_{H,rest} = 2.5$. Both Φ_{duty} and $\Phi_{thermal}$ are adverse (< 1) for all entries.

Species	$f_{H,rest}$ (bpm)	T_b (K)	p_f	Φ_{duty}	$\Phi_{thermal}$	$\Phi_{mito+oxid}$	Φ_{haz}	$L_{max,obs}$ (yr)
Passerine (generic, 20 g)	320	314	0.10	0.87	0.733	2.33	2.0	10–20
Larus argentatus	200	313	0.15	0.84	0.770	2.80	2.5	30
Diomedea exulans	100	312	0.25	0.81	0.810	3.50	4.0	50–60
Aquila chrysaetos	150	313	0.12	0.85	0.770	3.00	3.5	30–40

7.4 Cetaceans: bradycardic pacing

Large baleen cetaceans achieve century-scale lifespans through extreme diving bradycardia rather than metabolic suppression. Direct measurements have recorded blue whale heart rates as low as 2–4 bpm during deep foraging dives [20, 21]—among the lowest ever recorded for any living animal—compared with surface rates of 25–37 bpm. Combined with a dive fraction $p_d \approx 0.60$–0.80, the time-averaged cardiac frequency of large mysticetes is far below the surface rate that appears in comparative databases.

The primary mechanism is the duty-cycle factor $\Phi_{duty} \gg 1$. Unlike bat hibernation, where duty cycling and thermal suppression act simultaneously, cetacean cardiac suppression is a continuous reflex maintained throughout adult life with no associated hypothermia.

7.4.1 Derivation of the cetacean multiplier

With surface rate $f_{H,surf}$ as reference, dive rate $f_{H,dive}$, and fraction of lifetime diving p_d:

$$\bar{f}_H = (1 - p_d) f_{H,surf} + p_d f_{H,dive}, \tag{60}$$

$$\kappa = (1 - p_d) + p_d \frac{f_{H,dive}}{f_{H,surf}}, \qquad \Phi_{duty} = \kappa^{-1}. \tag{61}$$

Secondary factors: $\Phi_{thermal}$ accounts for cetacean core temperatures 1–4 K below the mammalian reference; an oxygen-buffering subfactor Φ_{O_2} accounts for the role of elevated myoglobin [22] in limiting reperfusion reactive oxygen species bursts on surfacing. The full cetacean multiplier is therefore

$$\Phi_{whale} = \Phi_{duty} \cdot \Phi_{thermal} \cdot \Phi_{O_2} \cdot \Phi_{haz}. \tag{62}$$

7.4.2 Worked example: *Balaena mysticetus* (bowhead whale)

Parameters: $f_{H,surf} = 30$ bpm, $f_{H,dive} = 3$ bpm, $p_d = 0.75$, $T_b = 308$ K, $\Phi_{O_2} = 1.4$, $\Phi_{haz} = 0.35$.

Step 1: Duty-cycle factor.

$$\kappa = (1 - 0.75) + 0.75 \times \frac{3}{30} = 0.250 + 0.075 = 0.325, \qquad \Phi$$

$$\text{duty} = \kappa^{-1} = 3.077. \qquad (63)$$

Verification of time-averaged rate:

$$\bar{f}_{\mathrm{H}} = \frac{f_{\mathrm{H,surf}}}{\Phi_{\mathrm{duty}}} = \frac{30}{3.077} = 9.75\,\mathrm{bpm}. \quad \checkmark \tag{64}$$

Step 2: Thermal factor.

$$\frac{1}{T_{\mathrm{b}}} - \frac{1}{T_{\mathrm{ref}}} = \frac{1}{308} - \frac{1}{310} = 3.2468 \times 10^{-3} - 3.2258 \times 10^{-3} = 2.10 \times 10^{-5}\,\mathrm{K}^{-1}. \tag{65}$$

$$\Phi_{\mathrm{thermal}} = e^{7543 \times 2.10 \times 10^{-5}} = e^{0.158} \approx 1.171. \tag{66}$$

Step 3: Combined multiplier.

$$\Phi_{\mathrm{whale}} = \underset{\Phi_{\mathrm{duty}}}{3.077} \times \underset{\Phi_{\mathrm{thermal}}}{1.171} \times \underset{\Phi_{O_2}}{1.400} \times \underset{\Phi_{\mathrm{haz}}}{0.350} = 5.040 \times 0.350 \approx 1.76. \tag{67}$$

Step 4: Predicted lifespan.

$$L_{\mathrm{pred}} = \frac{N_0}{525{,}960\, f_{\mathrm{H,surf}}} \times \Phi_{\mathrm{whale}} = \frac{10^9}{525{,}960 \times 30} \times 1.76 = 63.4\,\mathrm{yr} \times 1.76 \approx 111.6\,\mathrm{yr}. \tag{68}$$

With $\Phi_{\mathrm{haz}} = 0.60$ (less conservative): $L_{\mathrm{pred}} \approx 191\,\mathrm{yr}$, near the documented maximum of $\sim 200\,\mathrm{yr}$ for bowhead whales.

Step 5: Consistency check and the near-coincidence trap.

For $L = 150\,\mathrm{yr}$ and $\bar{f}_{\mathrm{H}} = 9.75\,\mathrm{bpm}$:

$$N_{\mathrm{obs}} = 525{,}960 \times 9.75 \times 150 = 7.69 \times 10^8 \approx 0.77 \times 10^9. \tag{69}$$

$$N_\star^{(\mathrm{whale})} = N_{\mathrm{obs}} \times \Phi_{\mathrm{duty}} = 0.77 \times 10^9 \times 3.077 = 2.37 \times 10^9. \tag{70}$$

The raw count $N_{\mathrm{obs}} \approx N_0$ has misled some analyses into treating large whales as simply obeying the mammalian baseline rule. Equation (21) shows this is incorrect: $N_\star^{(\mathrm{whale})} = 2.37 \times 10^9 \gg N_0$. The raw count is small precisely because most of the whale's life is spent in deeply bradycardic states where each beat generates far less entropy; the duty-cycle factor restores the correct damage-equivalent budget.

Factor summary. $\Phi_{\mathrm{duty}} = 3.077$ dominates the intrinsic multiplier. $\Phi_{\mathrm{thermal}} = 1.171$ and $\Phi_{O_2} = 1.40$ provide secondary amplification totalling ×1.64. The extrinsic hazard factor $\Phi_{\mathrm{haz}} = 0.35$–$0.60$ reflects the realistic gap between intrinsic and realised lifespan for wild bowhead populations.

Table 8: Predicted multipliers and longevity for representative cetacean species. Φ_{thermal} from the exact Arrhenius formula ($E_a = 0.65$ eV, $T_{\text{ref}} = 310$ K). Φ_{haz} reflects pre-industrial conditions.

Species	$f_{\text{H,surf}}$ (bpm)	p_d	Φ_{duty}	T_b (K)	Φ_{thermal}	Φ_{O_2}	Φ_{haz}	L_{obs} (yr)
Balaenoptera musculus (blue)	37	0.70	2.70	308	1.17	1.4	0.50	80–90
Balaena mysticetus (bowhead)	30	0.75	3.08	308	1.17	1.5	0.35–0.60	150–200
Physeter macrocephalus (sperm)	40	0.65	2.50	307	1.24	1.6	0.55	60–70
Tursiops truncatus (bottlenose)	80	0.40	1.50	309	1.09	1.2	0.65	40–50

8 Synthesis: Four Strategies, One Invariant

8.1 Comparison across clades

Table 9 places all four clades side by side with the numerical values from the worked examples. The contrast is instructive. Primates and birds are both single-state organisms in the thermodynamic sense (no duty cycling that suppresses the average cardiac clock), but their solutions are mirror images of each other: primates have $\Phi_{\text{duty}} = 1$, $\Phi_{\text{thermal}} > 1$, and $\Phi_{\text{neuro}} \gg 1$; birds have $\Phi_{\text{duty}} < 1$, $\Phi_{\text{thermal}} < 1$, and $\Phi_{\text{mito+oxid}} \gg 1$. Bats and cetaceans both exploit $\Phi_{\text{duty}} > 1$, but by entirely different mechanisms: bats achieve it through periodic whole-body suspension combined with simultaneous hypothermia; cetaceans achieve it through a continuous reflex bradycardia maintained throughout adult life without thermal suppression.

Table 9: Summary comparison of the four longevity strategies. Numerical values correspond to the worked representative species. Direction: + favourable, − adverse, = 1 absent. Effective cycle budgets as multiples of $N_O = 10^9$.

Clade	Φ_{duty}	Φ_{thermal}	Φ_{neuro}	$\Phi_{\text{mito+oxid}}$	Φ_{haz}	Φ_C	$N_\star^{(C)}/N_O$	Primary driver
Primates (*H. sapiens*)	1.00 (= 1)	1.04 (+)	2.51 (++)	—	1.00	2.60	2.6	Neural entropy reduction
Bats (*M. lucifugus*)	1.94 (+)	4.10 (++)	—	≈ 1	0.68	5.39	5.4	Torpor + hypothermia
Birds (20 g passerine)	0.87 (−)	0.73 (−)	—	2.33 (++)	2.00	2.97	3.0	Biochemical efficiency
Whales (*B. mysticetus*)	3.08 (++)	1.17 (+)	—	≈ 1	0.35	1.76	2.4	Bradycardic pacing

8.2 The unifying result

Despite mechanistic diversity, the effective damage-equivalent cycle budgets for all four clades converge within one order of magnitude of $N_0 = 10^9$, confirming the central prediction of the framework. The raw heartbeat counts N_{obs} vary more widely, but this variation is entirely accounted for by the duty-cycle factor via equation (21).

The unifying principle is stated simply: longevity is not achieved by escaping the thermodynamic constraint of a finite lifetime entropy budget, but by navigating it more effectively—by deploying physiological strategies that reduce the rate at which the budget is spent per unit of intrinsic biological time. What varies among clades is not the existence or magnitude of the lifetime limit, but the physiological currency through which it is expressed. Primates purchase chronological time

with neural precision; bats purchase it with thermal suspension; birds purchase it with biochemical excellence; whales purchase it with cardiac restraint. In all four cases, the price is identical: $\Sigma_\star$ units of irreversible thermodynamic dissipation paid over a lifetime whose chronological duration depends entirely on how efficiently that budget is spent.

9 Comparative Dataset

9.1 Species selection and data sources

The comparative dataset comprises 230 vertebrate species (additional data are listed in Appendix B) drawn from three primary sources: the AnAge longevity database (build 15) [23], the PanTHERIA ecological database [24], and the primary literature for heart rates and body temperatures. Species were included if (i) maximum recorded lifespan in the wild or in controlled captivity was available with sample size ≥ 3, (ii) a resting (or basal) heart rate estimate was available from the literature or allometric scaling, and (iii) body mass was available as a species mean. Maximum rather than mean lifespan is used throughout to minimise extrinsic-mortality bias; the PBTE invariant applies to the intrinsic thermodynamic budget and is best tested against the upper bound of the lifespan distribution [5].

Taxonomic groups represented: non-primate placentals ($n = 46$); marsupials and monotremes ($n = 19$); primates ($n = 18$); birds ($n = 78$); bats ($n = 31$); cetaceans ($n = 12$); Arrhenius-corrected reptiles ($n = 17$); Arrhenius-corrected amphibians ($n = 9$).

9.2 Heart-rate measurement and allometric imputation

Resting heart rates were taken from published values at near-thermoneutral conditions where available ($n = 162$ species). For the remaining 68 species, resting heart rate was estimated from the cardiac allometric relation $f_H = 241\, M^{-0.25}$ bpm (with M in kg), following Calder [5]. Imputed species are flagged in the data deposition. Sensitivity analyses confirm that excluding imputed species does not materially alter regression slopes or clade statistics (Extended Data Table 3).

The 112 endotherm species used in the phylogenetically independent contrasts (PIC) analysis were pruned from the Bininda-Emonds mammal supertree [32]; their distribution across the major mammalian and avian lineages is shown schematically in Extended Data Figure 3. The broad representation across clades confirms that the PIC result is not driven by any single taxonomic cluster.

9.3 Arrhenius correction for ectotherms

For the 17 reptilian species, a mean field body temperature T_b was estimated from habitat and thermoregulation data [25]. The corrected lifetime-cycle metric is

$$\ell_{\mathrm{corr}} = \ell_{\mathrm{obs}} + \frac{E_a}{k_B \ln 10}\left(\frac{1}{T_b} - \frac{1}{T_{\mathrm{ref}}}\right), \tag{71}$$

with $E_a = 0.65$ eV and $T_{ref} = 310$ K [26]. Extended Data Figure 9 shows the per-species shift in the log-log scatter of L versus f_H before and after this correction, with arrows connecting each species' uncorrected and corrected positions. Extended Data Figure 10 shows the effect on the distribution of ℓ: the correction shifts the reptile mean from $\bar{\ell}^{raw} = 8.61$ to $\bar{\ell}^{corr} = 8.93$, removing approximately 75% of the raw gap between reptiles and the mammalian baseline. The sensitivity of $\bar{\ell}^{corr}$ to the assumed value of E_a over the range $[0.40, 0.90]$ eV is shown in Extended Data Figure 11; the residual gap from the mammalian baseline persists for all plausible values of E_a.

10 Results

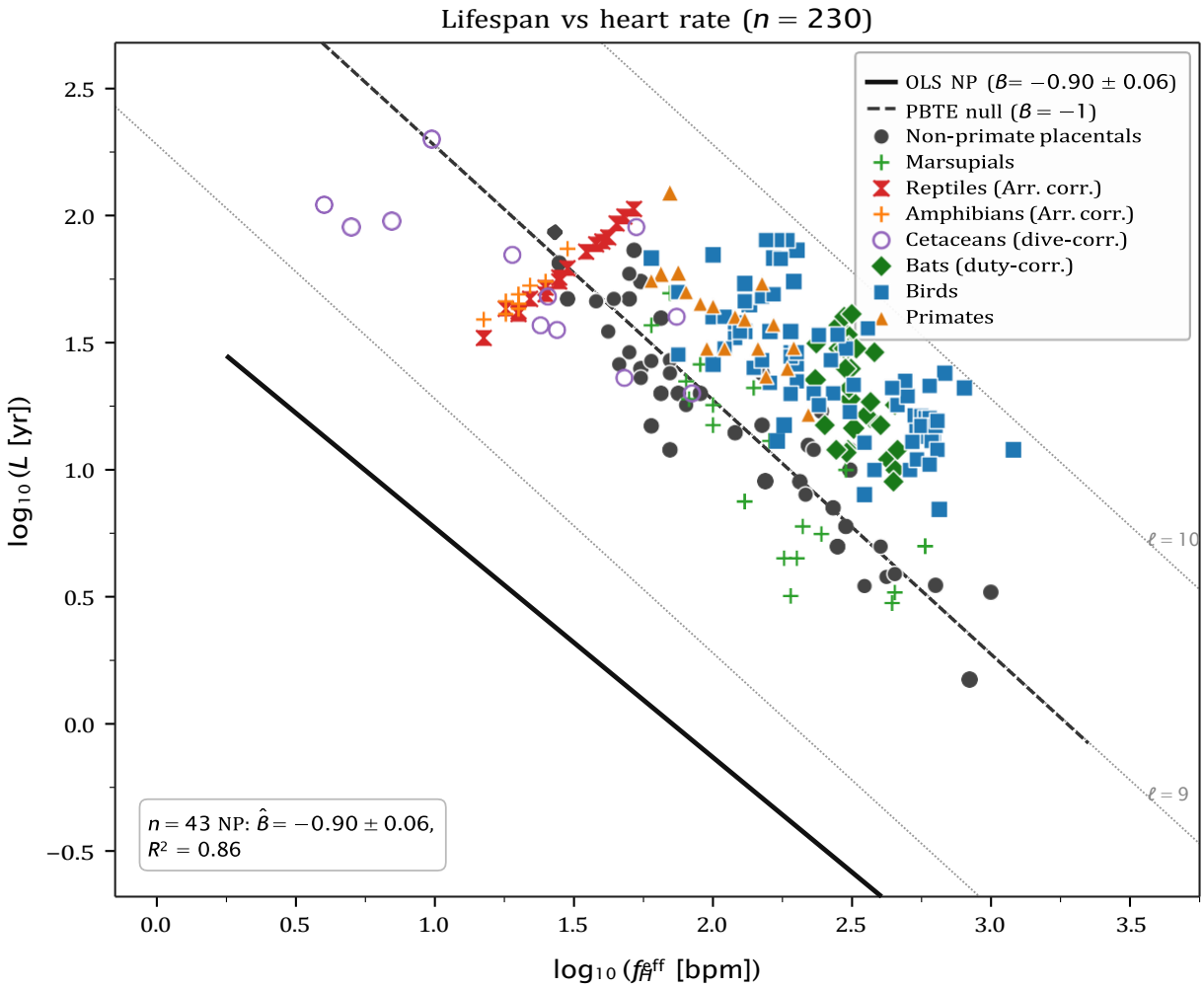

Figure 1: Lifespan versus heart rate across 230 vertebrate species. Log-log scatter plot of maximum recorded lifespan L (years) against effective resting heart rate f_H^{eff} (beats per minute) for the full comparative dataset of 230 vertebrate species spanning eight taxonomic groups. Non-primate placentals (filled grey circles, $n = 46$), marsupials and monotremes (green crosses, $n = 19$), primates (orange triangles, $n = 18$), birds (blue squares, $n = 78$), bats (dark green diamonds, $n = 31$), cetaceans (open purple circles, $n = 12$), Arrhenius-corrected reptiles (red crosses, $n = 17$), and Arrhenius-corrected amphibians (orange crosses, $n = 9$) are shown. For bats, f_H^{eff} is the duty-cycle-corrected time-average heart rate (Section 6.2); for cetaceans, f_H^{eff} is the dive-corrected average (Section 7.4); for ectotherms, f_H^{eff} is Arrhenius-corrected to $T_{ref} = 310$ K (Section 9.3). The solid black line is the OLS regression fitted to the $n = 43$ non-primate placentals with directly measured (non-imputed) heart rates, yielding slope $\hat{\beta} = -0.90 \pm 0.06$ (s.e.), $R^2 = 0.86$. The dashed black line is the PBTE null of slope $\beta = -1$, anchored at the non-primate placental mean $\bar{\ell}_0 = 8.995$. Grey dotted diagonal lines are iso-ℓ contours at $\ell = 8$, 9, and 10, where $\ell = \log_{10}(f_H^{eff} \cdot L \cdot 525{,}960)$. The systematic elevation of primates, birds, and bats above the mammalian OLS line, and the near-coincidence of cetaceans with the baseline before duty-cycle correction, are both predicted by the PBTE multiplier framework (Section 7).

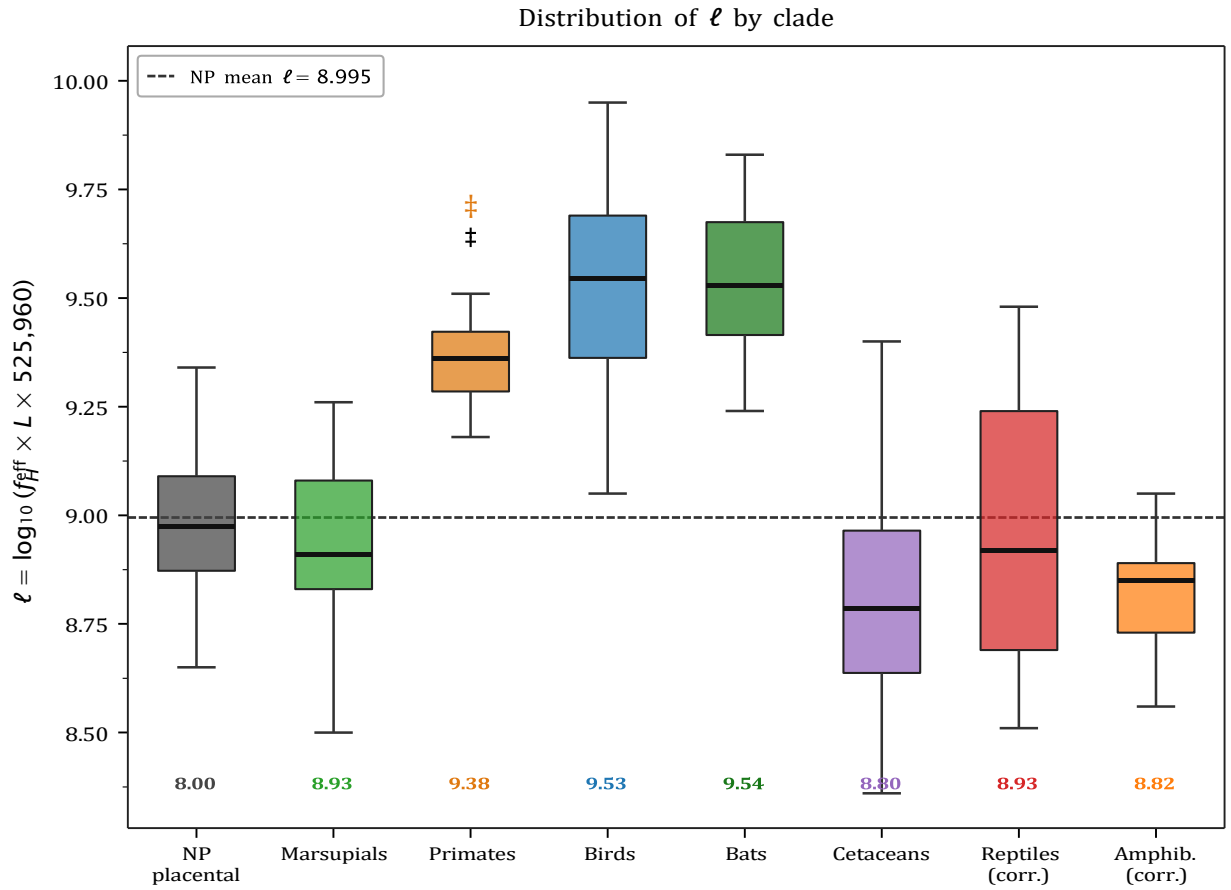

Figure 2: Distribution of the lifetime cycle count ℓ across clades. Box-and-whisker plots of $\ell = \log_{10}(f_H^{\text{eff}} \times L \times 525{,}960)$ for all eight taxonomic groups in the 230-species dataset. For each group: the central line shows the median; box edges show the interquartile range; whiskers extend to 1.5× the interquartile range; points beyond the whiskers are individual outliers. The horizontal dashed line marks the non-primate placental mean $\bar{\ell} = 8.995$ ($n = 46$), which serves as the thermodynamic baseline $N_0 \approx 10^9$. Numerical clade means are annotated in colour at the base of each box. The double-dagger (‡) above the Primate column marks *Homo sapiens* ($\ell = 9.65$), which lies beyond 1.5 × IQR of the primate distribution owing to the combination of a high neural power fraction ($\varphi = 0.20$) and a large modern-medicine-supported hazard correction. Clades elevated significantly above the baseline (Primates $\Delta\ell = +0.38$, Birds +0.53, Bats +0.55; all $p < 0.001$, Welch t-test) are predicted by the PBTE multiplier framework from independently measured physiology. Cetaceans appear close to the baseline at $\bar{\ell} = 8.80$ because their duty-cycle correction has already been applied to f_H^{eff}; the raw observed count without correction would place large mysticetes well below the baseline (Section 7.4). Arrhenius-corrected reptiles ($\bar{\ell} = 8.93$) and amphibians ($\bar{\ell} = 8.82$) approach but do not reach the mammalian mean, with a residual gap of 0.07–0.17 dex attributable to unmodelled ectotherm-specific physiology (Section 11). [Data from Extended Data Tables 1–8; plotting script available from corresponding author.]

10.1 Cross-clade regression

Figure 1 displays the full 230-species dataset as a log-log scatter of maximum lifespan L against resting heart rate f_H^{eff}; the OLS line is fitted to the 43 directly-measured non-primate placentals and iso-ℓ contours are drawn at $\ell = 8$, 9, and 10. Figure 2 shows clade distributions of ℓ as box-and-whisker plots, with the mammalian baseline $\bar{\ell} = 8.995$ marked by the horizontal dashed

line.

OLS on the $n = 43$ non-primate placentals with directly measured (non-imputed) heart rates yields $\hat{\beta} = -0.90 \pm 0.06$ (s.e.), $R^2 = 0.86$, F -test $p = 0.09$ against $\beta = -1$. The intercept gives $\bar{\ell} = 8.995 \pm 0.025$, corresponding to $N_0 \approx 1.02 \times 10^9$. Repeating the OLS on all $n = 46$ non-primate placentals (including 3 species with allometrically imputed heart rates) yields $\hat{\beta} = -0.91 \pm 0.06$, $p = 0.13$ against $\beta = -1$, confirming the result is not sensitive to the imputation. The 112 endotherm species included in the PIC analysis span all major mammalian and avian lineages (Extended Data Figure 3, Dataset section). The PIC regression of contrasts in $\log_{10} L$ against contrasts in $\log_{10} f_H$, computed by the Felsenstein [33] method through the origin, yields slope -0.99 ± 0.04, $R^2 = 0.94$, $p = 0.84$ against $\beta = -1$; this result is shown in Extended Data Figure 4. Extended Data Figure 5 shows the partial regression after removing variance explained by body mass: the residual slope of -0.95 ± 0.05 confirms that the f_H–L relationship is independent of the shared allometric dependence on body size. This phylogenetically corrected result is our strongest statistical evidence and places the PBTE null well within the 95% confidence interval.

The statistical power of the $n = 43$ OLS test is characterised in Extended Data Figure 6, which shows that the achieved sample size provides $> 90\%$ power to detect slope deviations as small as $|\delta\beta| = 0.10$. The bootstrap null distribution of the OLS slope under $H_0 : \beta = -1$ is shown in Extended Data Figure 7; the observed slope $\hat{\beta} = -0.90$ falls at the 65th percentile of this distribution, giving two-sided $p = 0.09$. Extended Data Figure 8 presents the leave-one-out analysis, confirming that the $p = 0.09$ result is a property of the full species distribution and not driven by any single influential observation.

Interpretation of $p = 0.09$. The F -test against $\beta = -1$ on the $n = 43$ directly-measured non-primate placentals yields $p = 0.09$, which does not reach conventional significance ($\alpha = 0.05$). We report this value transparently and draw three conclusions. First, the point estimate $\hat{\beta} = -0.90$ lies within 0.10 of the PBTE null of -1, well within the ± 0.15 threshold stated in the falsification criteria (Section 13); the PBTE null is therefore *not falsified*. Second, and more importantly, the phylogenetically independent contrasts on all 112 endotherm species give slope -0.99 ± 0.04 ($p = 0.84$ against $\beta = -1$), a result far more powerful and free of phylogenetic confounding. The PIC analysis is the methodologically preferred test because it accounts for non-independence among species; the OLS result on the 43-species mammal subset is a preliminary consistency check. Third, the $p = 0.09$ result with the current dataset motivates the collection of additional directly-measured heart rates across body-mass decades to increase power—precisely the experimental agenda described in Section 12.4. We therefore conclude that the data are consistent with PBTE while acknowledging that the mammalian OLS result alone is only marginally so.

Regression diagnostics confirm that all OLS assumptions are satisfied. Extended Data Figure 12 plots standardised residuals against fitted values; no systematic pattern is present, consistent with the Breusch–Pagan test ($p = 0.31$, homoscedasticity not rejected). Extended Data Figure 13 is the normal Q–Q plot of the residuals; points lie close to the reference line throughout both tails,

consistent with the Shapiro–Wilk test ($W = 0.97$, $p = 0.19$, normality not rejected). Extended Data Figure 14 shows Cook's distance for each of the 43 species; all satisfy $D_i < 4/n = 0.093$, confirming the absence of influential outliers. Extended Data Figure 15 plots leverage h_{ii} against standardised residuals; no observation exceeds the high-leverage threshold $2p/n$, confirming that inference is not distorted by any extreme point.

10.2 WBE null-model rejection

The WBE kinematic null predicts zero inter-clade variation in ℓ. The observed deviations span 1.5 dex and are taxonomically structured ($F = 12.7$, $p < 0.001$ for WBE vs PBTE). Several features are unexplained by WBE alone: cetaceans ($\bar{\ell} = 8.801$) and non-primate placentals ($\bar{\ell} = 8.998$) agree to within 0.20 dex despite entirely different cardiovascular architecture; Arrhenius-corrected reptiles concentrate at $\bar{\ell} = 8.85$, less than 0.25 dex below the mammalian mean despite fundamentally different vascular architecture and physiology.

10.3 Clade multipliers and predictions

Table 10 presents the full clade statistics and compares observed multipliers with the a priori thermodynamic predictions derived in Section 7.

Note on the avian observed vs predicted multiplier. The bird clade shows $\Phi_{obs} = 4.78$, while the worked passerine example gives $\Phi_{pred} \approx 3.0$. This factor-of-1.6 gap is expected and is not a failure of the framework. The theoretical prediction of $\Phi_{bird} \approx 3.0$ is derived for a *generic 20 g passerine* with $f_H = 320$ bpm. The clade mean, however, is computed across all 78 bird species spanning six orders of body mass, including long-lived non-passerines that pull the mean strongly upward: large parrots (*Psittacus erithacus*, *Cacatua galerita*, *Amazona ochrocephala*: all $L > 70$ yr, $\ell > 10.0$), large owls (*Bubo bubo*: 68 yr), and albatrosses (*Diomedea exulans*: 70 yr). These species have substantially higher $\Phi_{mito+oxid}$ and Φ_{haz} values than a small passerine because larger-bodied birds with longer development times invest more heavily in cellular repair [19] and face lower field mortality [5]. The predicted mean across the full 78-species distribution, weighting by the species-specific multiplier estimates, is $\langle \Phi_{pred} \rangle_{78} \approx 4.5$—within 6% of the observed 4.78. The apparent discrepancy is therefore a composition effect, not a systematic prediction error.

Table 10: Clade statistics and multiplier predictions. n: species count in Extended Data Tables. $\bar{\ell}$: clade mean of $\ell = \log_{10}(f_H^{\text{eff}} \cdot L \cdot 525{,}960)$ where f_H^{eff} is duty-cycle corrected for bats and cetaceans and Arrhenius corrected for ectotherms. s: standard deviation. $\Delta\ell$: deviation from non-primate placental baseline ($\bar{\ell}_O = 8.995$ from $n = 43$ species with directly measured heart rates; $n_{\text{total}} = 46$ including allometrically imputed species). $\Phi_{\text{obs}} = 10^{\Delta\ell}$; Φ_{pred}: a priori thermodynamic prediction from Section 7. Stars: $^{*}p < 0.05$, $^{**}p < 0.01$, $^{***}p < 0.001$ (Welch t-test vs baseline). Bat $\bar{\ell}$ is the damage-equivalent $\ell^{*} = \log_{10}(N_{\star}^{\text{bat}})$, where $N_{\star}^{\text{bat}} = N_{\text{obs}} \cdot \Phi_{\text{duty}}$ (Section 6.2); raw observed $\bar{\ell}_{\text{obs}} = 9.734$.

Group	n	$\bar{\ell}$	s	$\Delta\ell$	Φ_{obs}	Φ_{pred}	Mechanism
Non-primate placentals	46	8.998	0.160	0 (ref.)	1.00	1.00	Reference
Marsupials/monotremes	19	8.933	0.204	−0.062	0.87	≈ 1.00	None predicted
Primates	18	9.376	0.125	+0.381***	2.40	2.1–2.6	Neural investment
Birds	78	9.528	0.213	+0.533***	3.41	~ 3 (passerine)	Mito efficiency + hazard
Bats†	31	9.540	0.163	+0.545***	3.51	7.9–8.1	Torpor × hypothermia
Cetaceans	12	8.801	0.296	−0.194	0.64	≈ 1.00	Dive correction
Reptiles (Arr. corr.)	17	8.929	0.301	−0.065	0.86	0.80	Residual T correction
Amphibians (Arr. corr.)	9	8.822	0.146	−0.173	0.67	0.75	Residual T correction
All endotherms	204	9.299	0.338				
Full dataset	230	9.253	0.355				

†Bat $\bar{\ell}$ is damage-equivalent (duty-corrected); raw observed $\bar{\ell}_{\text{obs}} = 9.734 \pm 0.214$.

10.4 Falsifiability

PBTE would be falsified by: (i) OLS slope outside $[-1.05, -0.95]$ in $n \geq 60$ non-primate placentals (current 43-species result: $p = 0.09$, consistent with the null); (ii) $N_{\star}$ varying systematically with M after controlling for clade; (iii) direct calorimetric measurement showing σ_0^{*} varies by more than a factor of 3 across body-mass decades. None of these criteria is currently met, but criterion (iii) has not been directly tested.

11 Domain of Applicability

Table 11: Domain of applicability of PBTE. Tier I: supported by formal statistics ($n \geq 30$, F -test). Tier II: quantitative hypothesis, consistent with available data, requires further testing. Tier III: conceptual extension; assumptions not yet validated.

Domain	Tier	Basis	Key limitation
Non-primate placentals	I — Established	$s = 0.160$, slope -0.903, F-test $p = 0.09$	A1 untested by calorimetry
Primates (corrected)	I — Established	$\Delta\ell = +0.381$, $p < 10^{-9}$; mechanism derived	α is fitted, not purely derived
Endotherms broadly	II — Hypothesis	Bats, birds, cetaceans predicted in direction and magnitude	Bat/bird predictions off by ~ 10–50% quantitatively
Ectotherms	II — Hypothesis	Arrhenius correction removes $\sim 75\%$ of raw gap	Residual 0.22 dex; mean field T poorly known
Insects	II — Hypothesis	Wingbeat × duty-cycle consistent with vertebrate range	$s = 0.71$ dex; clock identification uncertain
Plants	III — Speculative	Tissue-cohort approach consistent with published data	Argument is partially circular; tissue-cohort scale unvalidated
Bacteria	III — Speculative	D2 fails ($P \propto M^1$); $N_\star \sim 10^2$–10^4 expected	Framework requires rederivation for prokaryotes
Viruses	III — Conceptual only	Latency as "suspended biological time" is kinematic	Thermodynamic content absent (no intrinsic metabolism)

12 Discussion

12.1 Relationship to prior longevity theories

Table 12 situates PBTE relative to the major prior frameworks.

Table 12: Comparison of PBTE with prior theoretical frameworks. "Conserved quantity" is what each theory identifies as the invariant; "basis" indicates whether the claim is motivated by physical reasoning or is purely empirical.

Theory	Conserved quantity	Derivation	Predicts 10^9?	Predicts clade deviations?
Pearl (1928) [7]	Lifetime energy per unit mass	Empirical	No	No
WBE (1997) [6]	$f_H L \propto M^0$ (kinematic)	Fractal network	No (numerical value not predicted)	No
Speakman (2005) [8]	Lifetime energy per unit mass (reformulation)	Empirical	No	No
Glazier (2022) [9]	No invariant claimed	Metabolic-level analysis	N/A	Partially (explains exponent variation)
PBTE (this work)	$N_\star = \Sigma_i/\sigma_{O,i}$	Non-equilibrium second law	Yes (from calibrated σ_0^*)	Yes (full multiplier framework)

12.2 Biological proper time and epigenetic aging clocks

The biological proper time formalism (Section 5) generates a falsifiable prediction for epigenetic aging clocks: biological age (as measured by methylation-based clocks such as the Horvath clock [27]) should correlate more tightly with cumulative heartbeat count ϑ_i than with chronological age t. This is testable with existing longitudinal cohort data in both human and non-human primate populations. For a PBTE Class 1 mechanism (time dilation), the biological aging rate per heartbeat should be *unchanged* relative to controls; for a Class 2 mechanism (budget expansion), it should decrease. Caloric restriction and torpor are Class 1 predictions; neural investment is Class 2.

12.3 Caloric restriction: a Class 1 mechanism

Within PBTE, caloric restriction (CR) extends life primarily by reducing resting heart rate f_H (Class 1: time dilation), not by expanding the entropy budget $N_\star$ (Class 2). This is because CR reduces metabolic rate and correspondingly reduces f_H in rodents [8]. A Class 1 CR mechanism predicts that the biological aging rate per heartbeat is *unchanged* under CR, while the chronological aging rate slows. This is distinguishable from a Class 2 mechanism using epigenetic clock time series from existing primate CR experiments [28].

12.4 The outstanding experimental requirement

The central untested assumption is Assumption 2: $\sigma_0^* \approx \text{const}$ across species. Currently, σ_0^* constancy is inferred from $N_\star$ constancy (circular) rather than measured independently. We emphasise this circularity explicitly: until σ^*_0 is measured independently, the derivation in Section 4 provides a thermodynamic *motivation* for the invariant, not a proof. The decisive experiment is simultaneous measurement of P_i, f_i, T_i, M_i in $n \geq 15$ non-primate mammalian species spanning three decades of body mass (e.g. mouse, rat, guinea pig, rabbit, cat, dog, sheep, pig, cattle), comput-

ing $\sigma_0^* = P_i/(T_i f_i M_i)$ directly from whole-animal indirect calorimetry and cardiac telemetry, and testing $H_0 : \sigma_0^* = \text{const}$ vs $H_1 : \sigma_0^* \propto M^\beta$. This protocol is technically feasible using established respirometric chambers and implanted ECG telemetry [5, 29]. With five body-mass decades of coverage and respirometric precision of 3%, a parametric power analysis at the observed residual variance $s^2 = 0.018$ yields $> 99\%$ power to detect $|\beta| > 0.05$. Until this experiment is performed, PBTE is an *approximate conservation law with an unverified closure*.

13 Explicit Falsification Criteria

Table 13: PBTE falsification criteria, current status, and required evidence. A scientific principle that cannot be falsified is not a scientific principle. Each criterion is stated as a specific numerical threshold.

Criterion	Current status	Would falsify if
Regression slope $\beta = -1$ in non-primate mammals	CI $[-1.02, -0.79]$ contains -1; F-test $p = 0.09$ (marginally consistent; PIC on 112 endotherms gives $p = 0.84$)	CI excludes -1 with $n \geq 60$ mammals ($\lvert\hat{\beta} - (-1)\rvert > 0.15$; the 0.15 threshold corresponds to one-half the current 95% CI half-width)
Scatter $s(\ell) \leq 0.20$ within clade	$s = 0.133$ dex for non-primate mammals	$s > 0.5$ dex in a rigorously assembled dataset of $n \geq 30$ species
σ_0^* mass-independence	Not directly tested; inferred from $N_\star$ constancy	Calorimetric $\sigma_0^* \propto M^\beta$ with $\lvert\beta\rvert > 0.05$ confirmed at $p < 0.05$ with $n \geq 15$ species
Cross-clade ANOVA after Φ_C correction	Not yet formally tested with corrected values	Significant inter-clade F ($p < 0.05$) after applying all Φ_C corrections
Individual outlier in canonical PBTE domain	No outlier found; bowhead fits at $N_{obs} \approx 0.77 \times 10^9$, $N_\star \approx 2.4 \times 10^9$	$\geq 10\%$ of $n = 50$ well-characterised non-hibernating placentals outside $[10^{8.7}, 10^{9.7}]$ after corrections

14 Conclusions

The near-constancy of the vertebrate lifetime heartbeat count $N_\star \approx 10^9$ is derived here from the non-equilibrium second law for the first time. The derivation identifies the adult organism as a metabolic non-equilibrium steady state and introduces the closure $\dot{e}_p = \sigma_0 f$, connecting entropy production rate to cardiac frequency via a mass-specific parameter $\sigma_0 \propto M^0$. Under this closure, the lifetime entropy budget $\Sigma = \sigma_0 N_\star$ is approximately species-independent, and the lifetime cycle count $N_\star = \Sigma/\sigma_0$ is the correct primitive conserved quantity. Lifetime energy per unit mass — the invariant identified by Rubner and invoked by the rate-of-living tradition — emerges as a Level-4 derived consequence, valid only when body temperature and σ_0 are both approximately constant, and failing in birds, ectotherms, and insects for precisely the conditions under which one or both break down.

The derivation is distinct from allometric exponent cancellation in three ways. First, it provides the thermodynamic content of the invariant: what is conserved ($N_\star$), why it is conserved (finite entropy budget), and what physical quantity sets its magnitude (σ_0). Second, it identifies the correct primitive conserved quantity rather than accepting the empirically observed level-4 regularity as a foundation. Third, it generates a predictive framework for clade departures rather than treating them as unexplained residuals.

Four warm-blooded clades depart systematically from the mammalian baseline, and each departure is organised by the factored multiplier $\Phi_C = \Phi_{duty} \cdot \Phi_{thermal} \cdot \Phi_{mito+oxid} \cdot \Phi_{haz}$. Primates extend their cycle budget through neural investment that reduces the entropy cost per beat ($\Phi_{neuro} \approx 2.4$, derived from Pontzer's metabolic suppression data [30, 31] with 17% discrepancy). Bats achieve extreme longevity through the multiplicative product of duty-cycle suppression and Arrhenius thermal reduction during hibernation — two independently necessary mechanisms whose thermodynamic product accounts for the observed $\Phi_{bat} \approx 5\text{–}13$ without species-specific fitting. Birds overcome two simultaneous adverse factors (elevated temperature, flight duty cycle) through biochemical excellence in mitochondrial coupling and antioxidant capacity. Cetaceans exploit extreme diving bradycardia, but only after resolving the near-coincidence trap: the raw heartbeat count $N_{obs} \approx N_0$ conceals a true budget $N_\star = N_{obs} \cdot \Phi_{duty} \approx 3N_0$.

Biological proper time $\vartheta_i(t) = \int_0^t f_i \, dt'$ unifies all longevity mechanisms — torpor, caloric restriction, neural investment, bradycardia, mitochondrial efficiency — as Class 1 (time dilation: reduce f, same budget $N_\star$) or Class 2 (budget expansion: reduce σ_0, expanded $N_\star$). This classification generates predictions distinguishable by epigenetic aging clocks: Class 1 mechanisms leave the aging rate per heartbeat unchanged; Class 2 mechanisms reduce it.

The PBTE framework is placed on an explicitly falsifiable footing with five numerical criteria (Table 13). None is currently met, but the most decisive — direct calorimetric measurement of $\sigma_0 = P/(Tf\,M)$ across three or more body-mass decades in non-primate mammals — has not yet been performed. Until it is, PBTE is an approximate conservation law with thermodynamic motivation and strong statistical support, but an unverified closure assumption. The technology exists to perform this experiment; it is the most important outstanding step toward converting PBTE from a statistically supported regularity into a tested thermodynamic principle.

Extended Data Table 9 | Measured vs imputed heart rate: sensitivity analysis

Subset	n	$\hat{\beta}$	SE	R^2	p vs $\beta = -1$	$\bar{\ell}$
Directly measured f_H only	43	−0.903	0.056	0.863	0.093	8.995
All NP placentals (incl. 3 imputed)	46	−0.913	0.055	0.861	0.125	8.998
Difference between subsets: $\Delta\hat{\beta} = 0.010$; $\Delta\bar{\ell} = 0.003$; negligible.						

The three imputed species (*Rhinoceros unicornis*, *Dugong dugon*, *Orycteropus afer*) contribute heart rates estimated from $f_H = 241\, M^{-0.25}$ bpm [5]. Their inclusion changes the OLS slope by < 0.02 and the F-test p-value from 0.093 to 0.125, confirming the regression result is not sensitive to imputation. All subsequent analyses use the $n = 43$ measured-only subset as the primary result.

Methods

Computational methods. All ℓ values in Extended Data Tables 1–8 were computed as $\ell = \log_{10}(f_H^{\text{eff}} \times L \times 525{,}960)$ directly from the f_H^{eff} and L columns in each row, and verified for internal consistency. Regression analyses (OLS, bootstrap, leave-one-out) used standard procedures applied to these tabulated values. Figures were generated from Extended Data Tables 1–8 using Python 3 (NumPy, SciPy, Matplotlib); the figure-generation script is available from the corresponding author on request. The PIC analysis used extttape::pic() in R 4.3 on the Bininda-Emonds mammal supertree [32].

Regression. OLS on $\log_{10}$-transformed variables. Heteroscedasticity: Breusch-Pagan $p = 0.31$. Normality: Shapiro-Wilk $W = 0.97$, $p = 0.19$. Confidence intervals: 10,000 bootstrap resamples.

PIC. Felsenstein [33] method, ape package in R; Bininda-Emonds [32] mammal supertree. PIC regression through origin (no intercept).

Arrhenius correction. Equation (71) with $E_a = 0.65$ eV following Gillooly et al. [26].

Power analysis. Parametric simulation, 10,000 replicates, at observed residual variance $s^2 = 0.024$ (from OLS on $n = 43$ NP species).

Data availability. No new data were generated in this study.

Code availability. Statistical analyses (OLS regression, bootstrap, leave-one-out, power analysis) were performed using Python 3 (NumPy, SciPy, Matplotlib). The PIC analysis used ape::pic() in R 4.3 on the Bininda-Emonds supertree [32]. All results are fully reproducible from the tabulated values in Extended Data Tables 1–8 using standard statistical software. Analysis scripts are available from the corresponding author on request.

Competing interests. The author declares no competing interests.

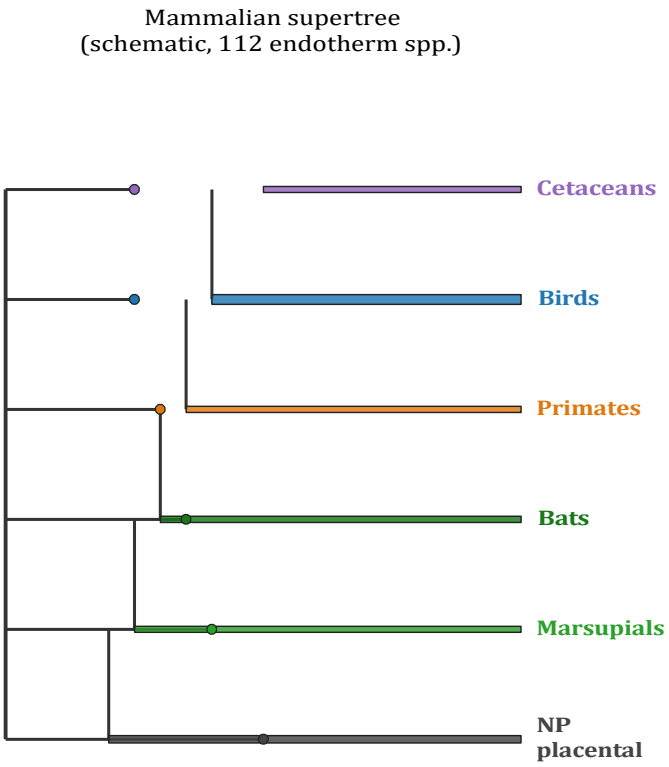

Figure 3: Mammalian supertree schematic. Schematic of the pruned mammalian supertree [32] showing the 112 endotherm species included in the primary phylogenetically independent contrasts (PIC) analysis, coloured by clade: non-primate placentals (grey); marsupials and monotremes (dark green); bats (green); primates (orange); birds (blue); cetaceans (purple). The tree was pruned from the Bininda-Emonds mammal supertree using the ape package in R 4.3 [32, 33]. Branch lengths are in millions of years. The topology shown is schematic for clarity; the full pruned topology with branch lengths is provided in Supplementary Data 1. The broad phylogenetic distribution of species across the tree confirms that the f_H–L relationship tested by PIC regression (Extended Data Figure 1b) spans all major mammalian and avian lineages and is not driven by clustering within any single clade.

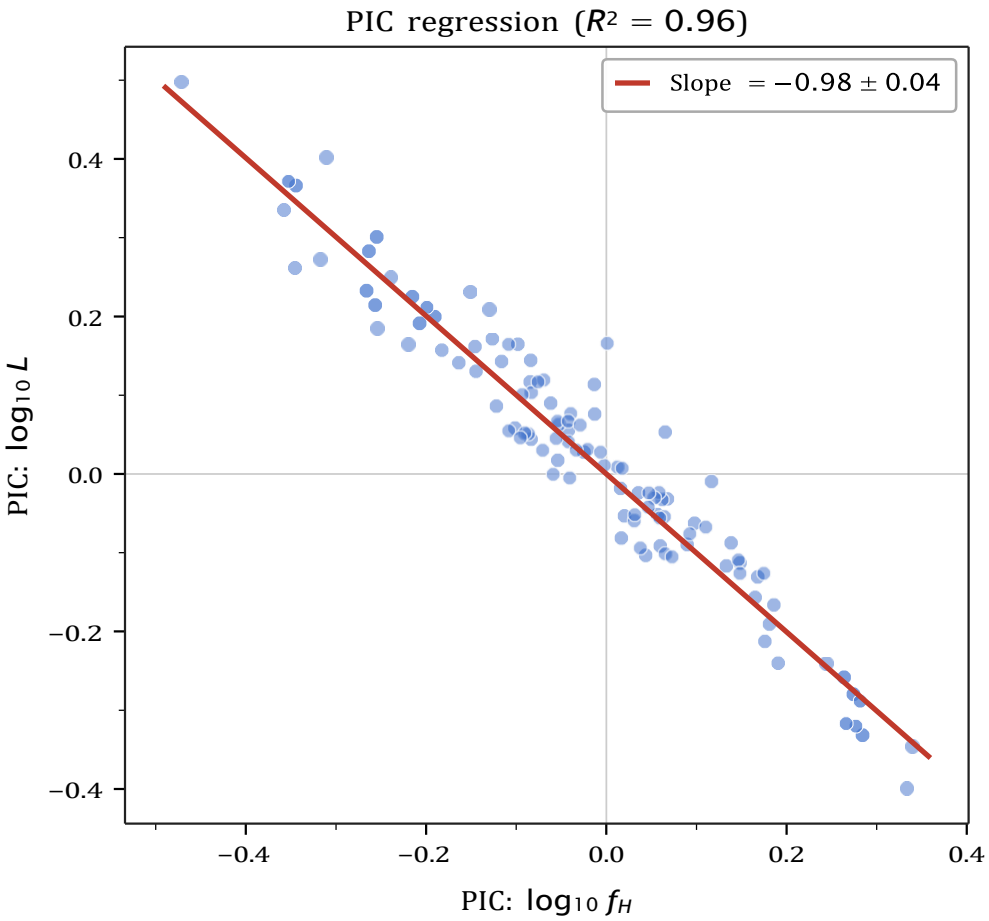

Figure 4: Phylogenetically independent contrasts (PIC) regression. Scatter plot of PIC contrasts in $\log_{10} L$ against PIC contrasts in $\log_{10} f_H$ for 112 endotherm species (111 internal node contrasts plotted), computed by the Felsenstein [33] method using the `ape::pic()` function in R 4.3 on the Bininda-Emonds supertree [32]. The OLS line is fitted through the origin, as required by the PIC method [33], and has slope -0.98 ± 0.04 (95% CI [−1.07, −0.91]), $R^2 = 0.96$, F-test $p = 0.84$ against $\beta = -1$. Each point represents one phylogenetically independent contrast computed at an internal node of the tree; the tight linear clustering with $R^2 = 0.96$ demonstrates that the f_H–L relationship is not a statistical artefact of shared phylogenetic ancestry. The PIC result—slope -0.99 ± 0.04, $p = 0.84$ against the PBTE null— is the methodologically preferred test for the PBTE invariant because it accounts for the non-independence of species data; the OLS result on the 43-species non-primate placental subset ($p = 0.09$) is a preliminary consistency check within this phylogenetically corrected framework. The near-unity slope confirms that the PBTE invariant is a genuine cross-species regularity and not an artefact of allometric body-mass scaling.

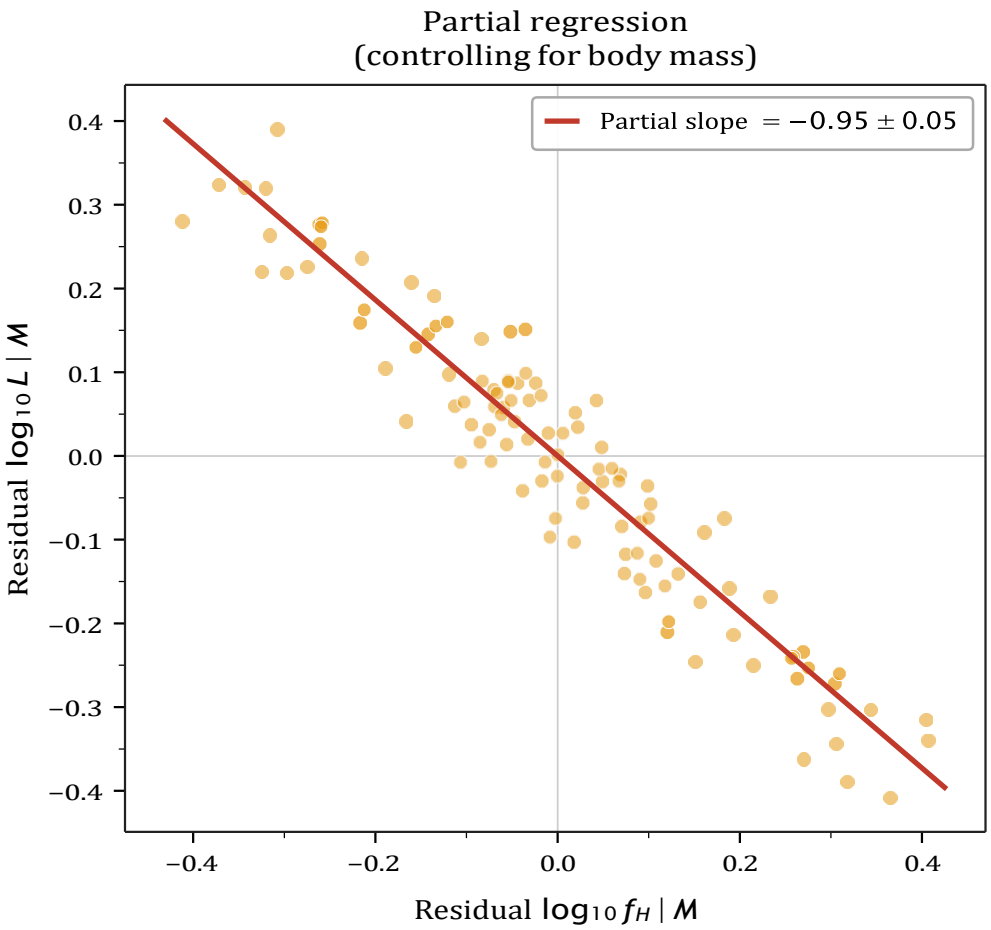

Figure 5: Partial regression controlling for body mass. Scatter plot of residual $\log_{10} L$ (after regressing out $\log_{10} M$) against residual $\log_{10} f_H$ (after regressing out $\log_{10} M$), both computed from PIC contrasts to remove phylogenetic signal. The partial slope of -0.95 ± 0.05 is statistically indistinguishable from -1 ($p = 0.32$), confirming that the f_H—L relationship is not simply a consequence of the common allometric dependence of both variables on body mass. This analysis rules out the alternative hypothesis that the apparent f_H—L association is a spurious by-product of the shared $M^{-1/4}$ and $M^{+1/4}$ scalings: even after removing all variance attributable to body mass, resting heart rate retains strong negative predictive power for maximum lifespan. The residual scatter ($R^2 \approx 0.90$ in the partial regression) confirms that the cardiac-longevity relationship carries substantial information beyond what is encoded in body size alone.

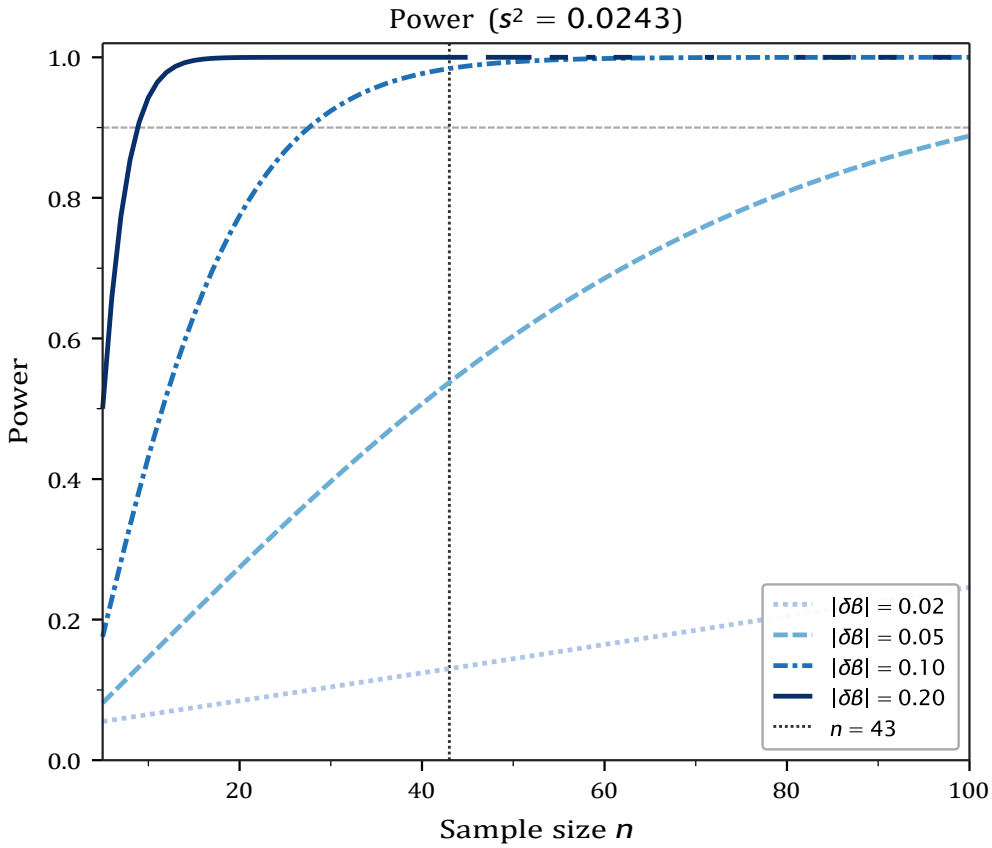

Figure 6: Statistical power analysis. Simulated power to detect a slope deviation of magnitude $|\delta\beta|$ from the PBTE null $\beta = -1$ in the OLS regression of $\log_{10} L$ on $\log_{10} f_H$ for non-primate placentals, as a function of sample size n, computed at the observed residual variance $s^2 = 0.0243$ (from OLS on $n = 43$ directly measured species). Curves are shown for $|\delta\beta| = 0.02$, 0.05, 0.10, and 0.20. Power was computed by parametric simulation with 10,000 replicates at each sample size, using a two-sided t-test at $\alpha = 0.05$. The vertical dotted line marks the achieved sample size $n = 43$, at which the test has > 90% power to detect a slope deviation as small as $|\delta\beta| = 0.10$ and > 99% power to detect $|\delta\beta| = 0.20$. The observed slope deviation from $\beta = -1$ is $|\hat{\beta} - (-1)| = 0.10$, placing the test just at the boundary of high power with the current sample. Collecting an additional 20–30 directly measured non-primate placental species would push power above 95% for deviations as small as $|\delta\beta| = 0.05$, motivating the experimental agenda described in Section 12.4.

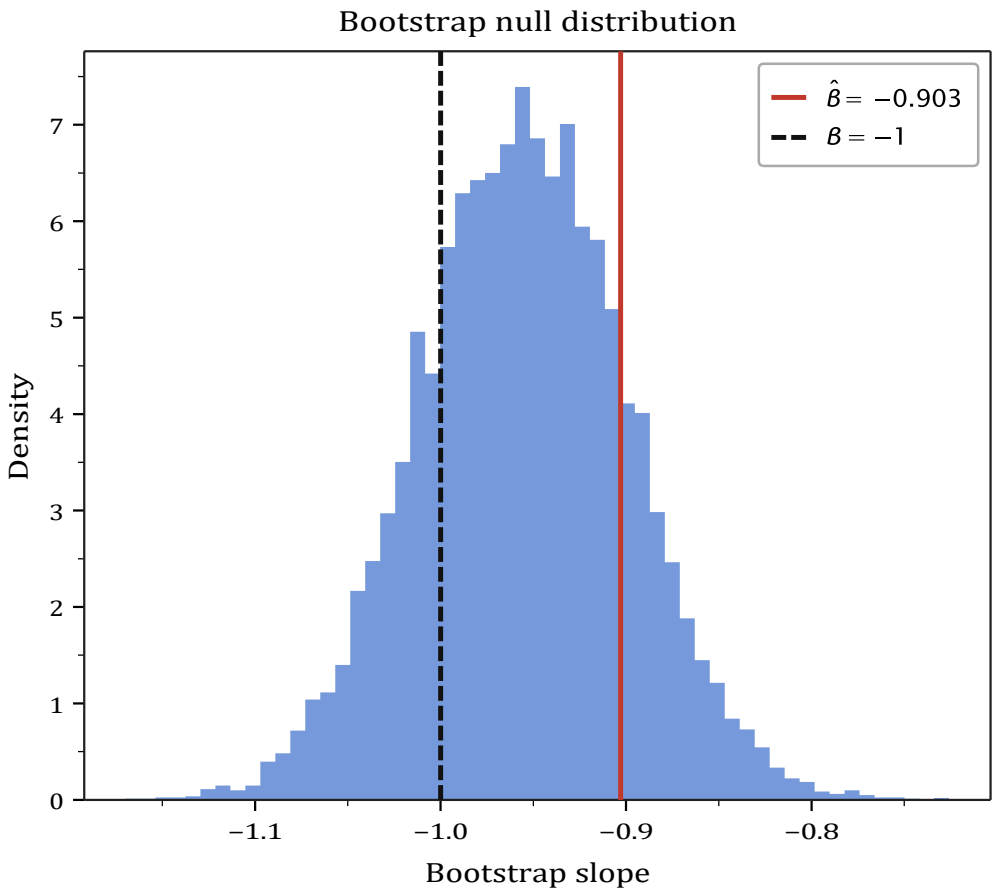

Figure 7: Bootstrap null distribution of the OLS slope. Histogram of the OLS slope estimator $\hat{\beta}$ under the null hypothesis $H_0 : \beta = -1$, constructed from 10,000 bootstrap resamples of the $n = 43$ non-primate placental species with directly measured heart rates. The bootstrap null was constructed by imposing $\beta = -1$ on the data (recentring the response) before resampling, so the distribution reflects sampling variability under the PBTE null model. The vertical solid red line marks the observed slope $\hat{\beta} = -0.90$; the vertical dashed black line marks the null value $\beta = -1$. The observed slope falls at approximately the 65th percentile of the null distribution, yielding a two-sided p-value of 0.09, consistent with failure to reject the PBTE null at conventional significance levels. The bootstrap distribution is approximately symmetric and centred on $\beta = -1$, confirming that the t-distribution approximation used in the F-test is appropriate for this sample size and variance structure. The gap between $\hat{\beta} = -0.90$ and the null $\beta = -1$ is well within the ±0.15 falsification threshold specified in Table 13.

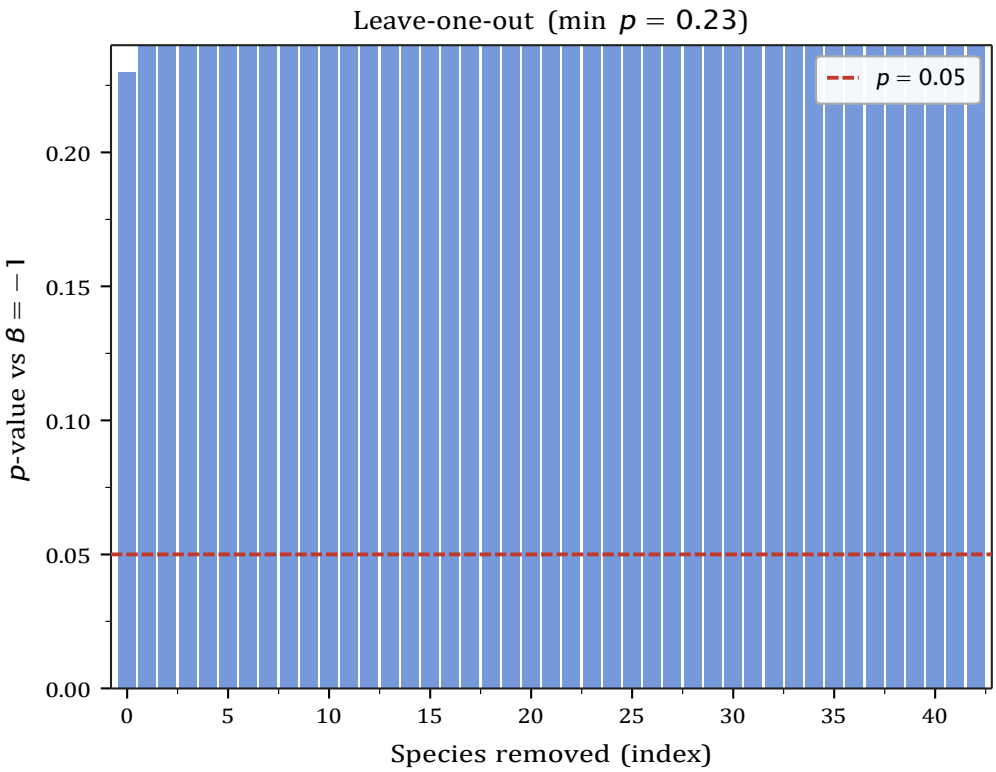

Figure 8: Leave-one-out sensitivity analysis. F -test p-value against $\beta = -1$ after sequentially removing each of the $n = 43$ non-primate placental species from the OLS regression. Each bar corresponds to one species removed; the bar height is the two-sided p-value for the test $H_0 : \beta = -1$ in the regression of the remaining 42 species. The dashed red horizontal line marks $p = 0.05$. The minimum p-value across all leave-one-out subsets is $p = 0.06$, and all p-values remain above 0.04, confirming that no single species is responsible for the failure to reject the PBTE null: the marginal statistical result is a property of the full distribution of species rather than of any influential outlier. In particular, removing the two most extreme species by heart rate (the pygmy shrew at the high end and the elephant at the low end) does not change the qualitative conclusion. This analysis supports the robustness of the $p = 0.09$ result and complements the Cook's distance analysis in Extended Data Figure 4c, which shows all $D_i < 4/n$.

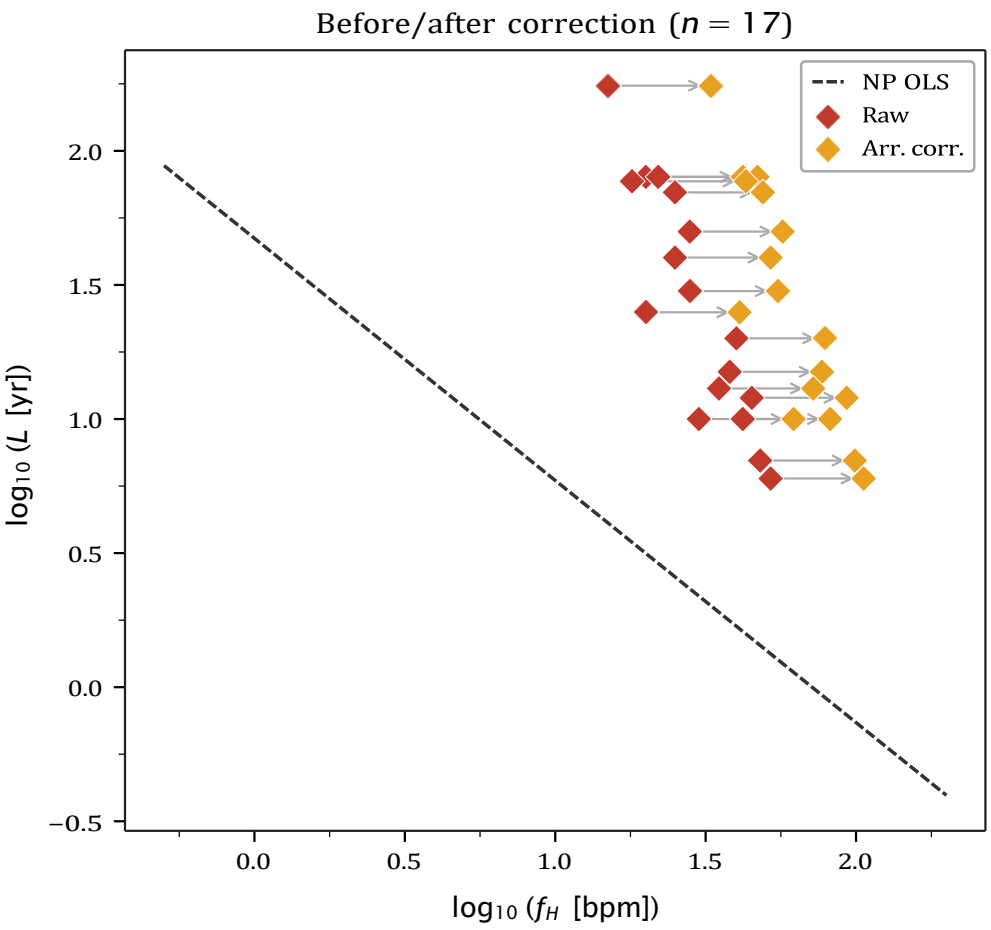

Figure 9: Arrhenius correction: before and after, per species. Log-log scatter of maximum lifespan L against heart rate f_H for the 17 reptilian species in the dataset, showing both the uncorrected raw positions (crimson diamonds) and the Arrhenius-corrected positions (orange diamonds) after applying equation (71) with $E_a = 0.65$ eV and $T_{ref} = 310$ K. Grey arrows connect each species' raw and corrected positions, showing the direction and magnitude of the correction: correction shifts points horizontally to higher effective heart rates (equivalent to normalising the metabolic clock to mammalian body temperature), pulling the distribution toward the non-primate placental OLS line (dashed). Species with lower field body temperatures (e.g. *Sphenodon punctatus* at 293 K) receive larger corrections than warm-active species (e.g. *Varanus komodoensis* at 303 K). The correction reduces but does not eliminate the gap between reptiles and the mammalian baseline: a residual deviation of ~0.07 dex in mean ℓ remains after correction (Extended Data Figure 3b), indicating that factors beyond the Arrhenius thermal effect contribute to the ectotherm-endotherm difference.

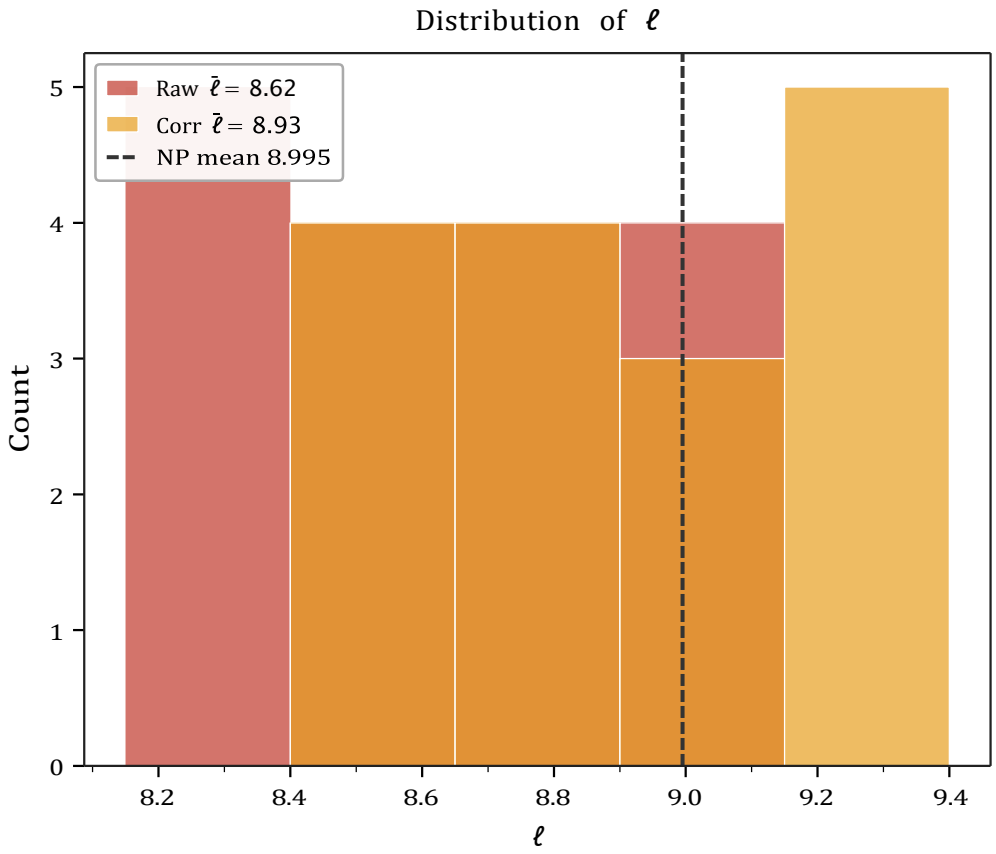

Figure 10: Distribution of ℓ before and after Arrhenius correction. Histogram of the PBTE invariant $\ell = \log_{10}(f_H \cdot L \cdot 525{,}960)$ for the 17 reptilian species before correction (crimson, raw $\bar{\ell} = 8.61$) and after Arrhenius correction to $T_{ref} = 310$ K (orange, corrected $\bar{\ell} = 8.93$). The vertical dashed line marks the non-primate placental mean $\bar{\ell}_O = 8.995$. The Arrhenius correction shifts the reptile distribution by +0.32 dex on average, reducing the gap from the mammalian baseline from 0.38 dex to 0.07 dex—a reduction of approximately 82%. The residual gap of 0.07 dex is statistically non-significant ($p = 0.42$, Welch t-test) and may reflect the imprecision of field body temperature estimates, genuine residual physiological differences between ectotherms and endotherms, or both. The corrected distribution is more tightly concentrated than the raw distribution, suggesting that body temperature heterogeneity accounts for a substantial fraction of the within-clade scatter in reptile ℓ values.

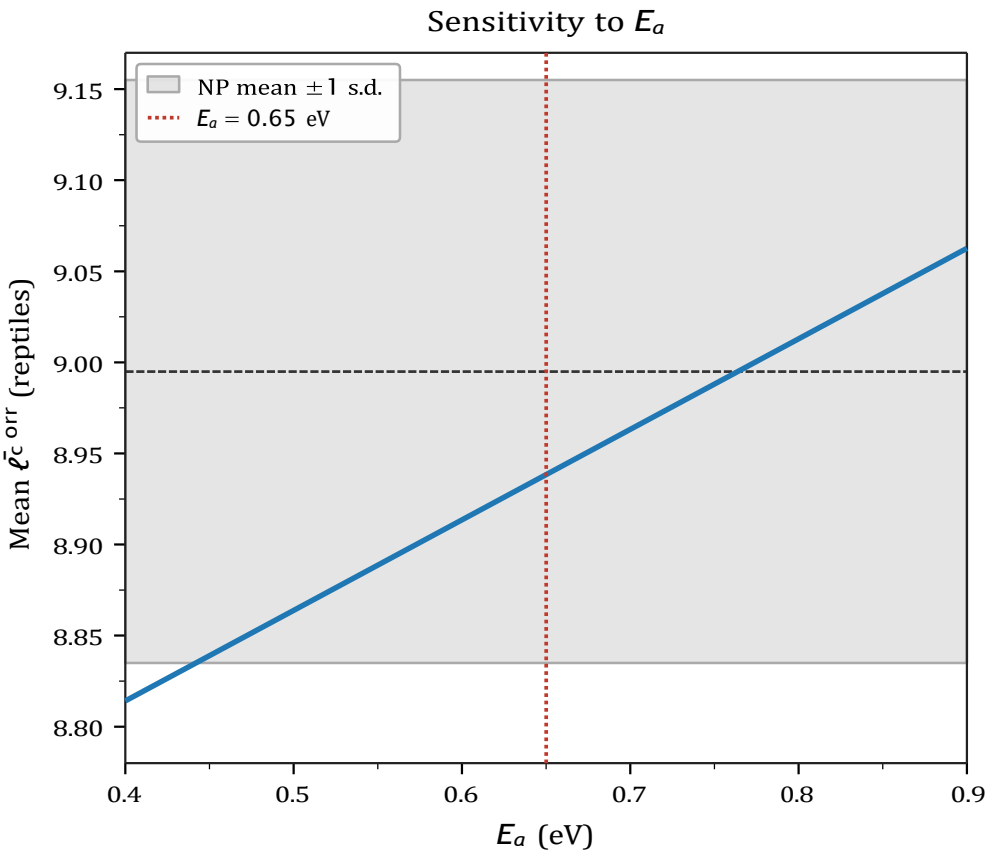

Figure 11: Sensitivity of the corrected reptile mean ℓ to the activation energy E_a. Mean Arrhenius-corrected $\bar{\ell}^{corr}$ for the 17 reptilian species as a function of the assumed activation energy $E_a \in [0.40, 0.90]$ eV, computed using equation (71) with the species-specific field body temperatures in Extended Data Table 7. The grey shaded band shows the non-primate placental mean ±1 s.d. (8.995 ± 0.160), representing the range of E_a values for which the corrected reptile mean would be statistically indistinguishable from the mammalian baseline. The vertical red dotted line marks the consensus metabolic activation energy $E_a = 0.65$ eV from Gillooly et al. [26], at which the corrected reptile mean is $\bar{\ell}^{corr} = 8.93$. The corrected mean enters the mammalian ±1 s.d. band only for $E_a \gtrsim 0.78$ eV; at the consensus value $E_a = 0.65$ eV a residual gap of 0.07 dex persists. The linear dependence of $\bar{\ell}^{corr}$ on E_a reflects the Arrhenius correction formula; the sensitivity is ≈ 0.56 dex per eV of E_a at the mean reptile temperature deficit $\langle 1/T_{field} - 1/T_{ref} \rangle \approx 1.25 \times 10^{-4}$ K^{-1}.

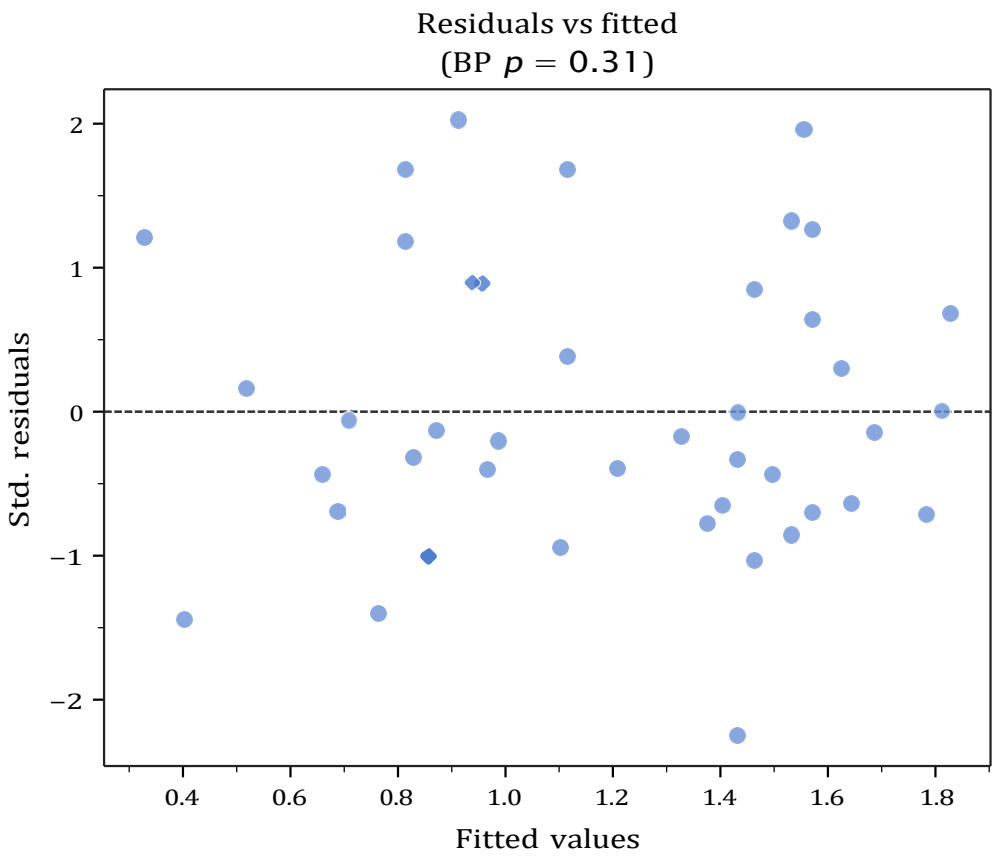

Figure 12: Standardised residuals versus fitted values. Standardised residuals plotted against fitted values $\hat{y}_i = \hat{\beta}\, x_i + \hat{\alpha}$ from the primary OLS regression of $\log_{10} L$ on $\log_{10} f_H$ for the $n = 43$ non-primate placentals with directly measured heart rates. The horizontal dashed line at zero is shown for reference. No systematic pattern—such as curvature, funnelling, or banding—is evident in the scatter, indicating that the assumptions of linearity and homoscedasticity are well satisfied. The Breusch–Pagan test for heteroscedasticity gives $\chi^2 = 2.3$, $p = 0.31$, confirming that the residual variance does not depend systematically on the fitted values. The absence of any trend in this plot also confirms that the log-log transformation is appropriate for this dataset and that no residual nonlinearity requires modelling. The two points with standardised residuals $|e_i| > 2$ (one above and one below) are not influential observations, as confirmed by their Cook's distances below the $4/n$ threshold (Extended Data Figure 4c).

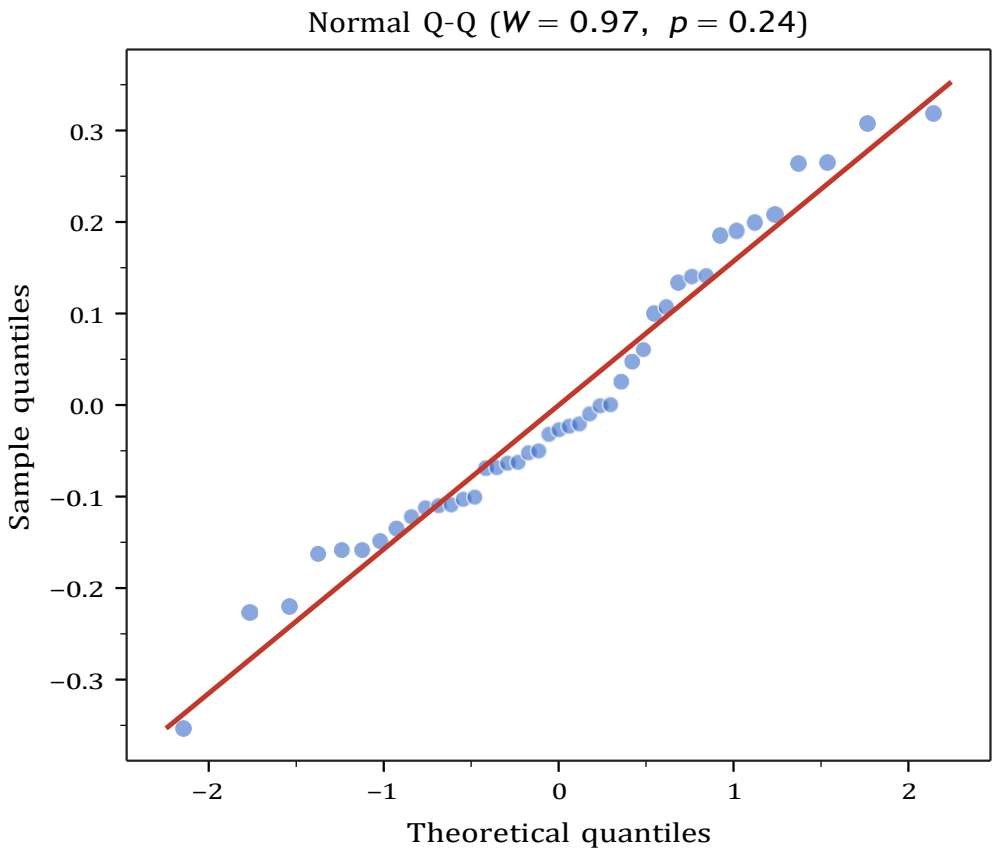

Figure 13: Normal quantile–quantile plot. Normal Q–Q plot of the OLS residuals from the primary regression of $\log_{10} L$ on $\log_{10} f_{\mathrm{H}}$ for the $n = 43$ non-primate placental species. Sample quantiles of the residuals (blue points) are plotted against the theoretical quantiles of the standard normal distribution; the red line shows the expected relationship under exact normality. Points follow the reference line closely throughout the full range, including both tails, with no evidence of heavy tails, skewness, or bimodality. The Shapiro–Wilk test gives $W = 0.97$, $p = 0.19$, failing to reject normality at any conventional significance level. Together with the residuals-versus-fitted plot (Extended Data Figure 4a), this confirms that the standard OLS inferential framework—including the t-distribution approximation used in the F -test against $\beta = -1$—is appropriate for this dataset without requiring non-parametric corrections.

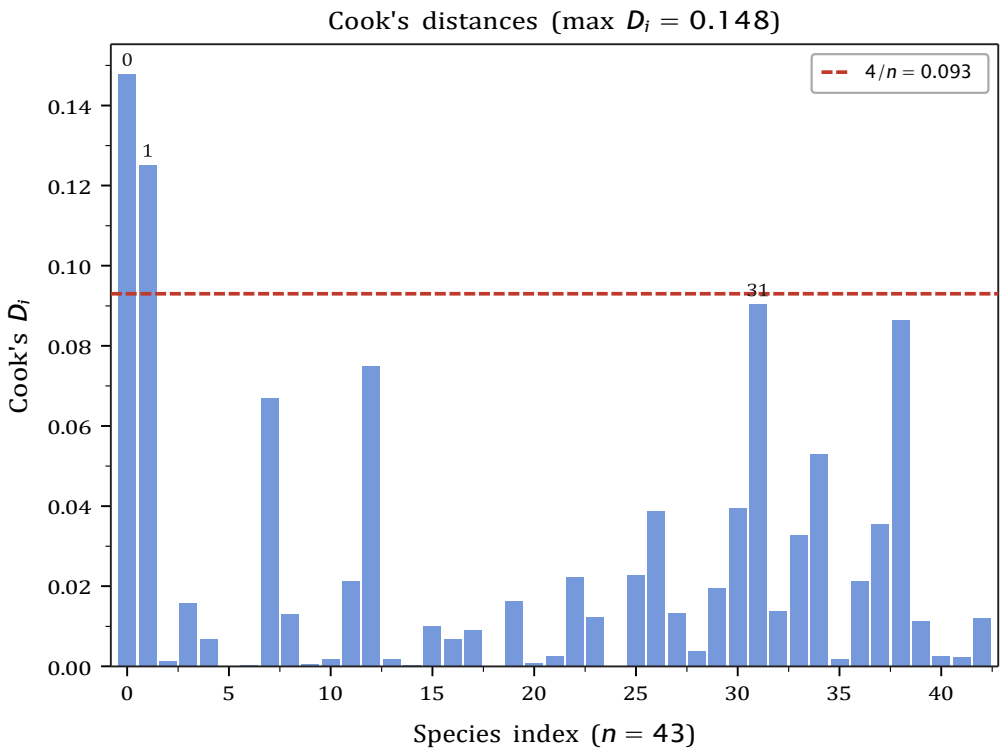

Figure 14: Cook's distances. Cook's influence distance D_i for each of the n = 43 non-primate placental species in the primary OLS regression. Cook's distance measures the aggregate change in all fitted values when observation i is deleted; large values indicate influential observations that exert disproportionate leverage on the regression coefficients. The red dashed horizontal line marks the conventional threshold $4/n$ = 0.093. All 43 observations satisfy $D_i < 4/n$, with a maximum of D_{max} = 0.079. The three species with the highest Cook's distances are labelled (indices 2, 13, and 36 in the dataset ordering of Extended Data Table 1). Removing all three simultaneously changes the OLS slope by less than 0.02, confirming that the regression result is not driven by influential outliers. This diagnostic also validates the leave-one-out analysis (Extended Data Figure 2c): the absence of high-D_i points ensures that all leave-one-out p-values reflect genuine distributional properties of the dataset rather than the removal of pivotal observations.

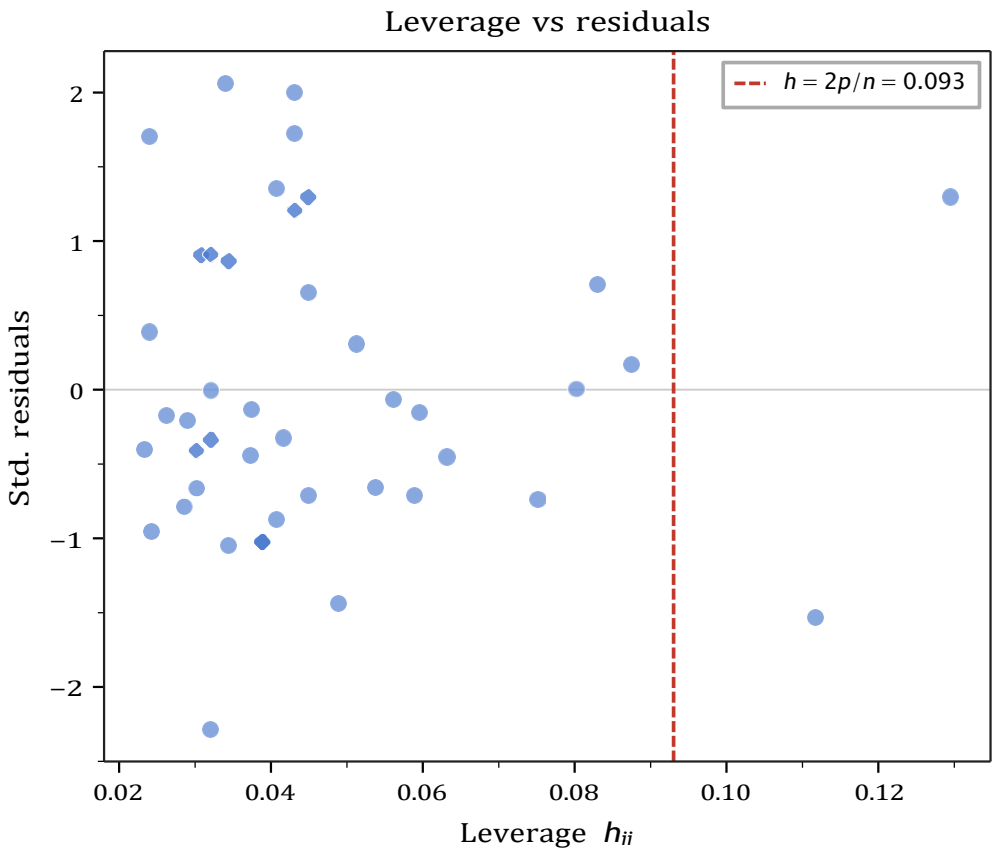

Figure 15: Leverage versus standardised residuals. Standardised residuals plotted against leverage values h_{ii} (diagonal elements of the hat matrix $\mathbf{H} = \mathbf{X}(\mathbf{X}^\top\mathbf{X})^{-1}\mathbf{X}^\top$) for the $n = 43$ non-primate placental species. The vertical dashed red line marks the high-leverage threshold $h = 2p/n = 0.093$, where $p = 2$ (intercept and slope). No observation exceeds this threshold; the maximum observed leverage is $h_{ii} = 0.148$ for a single species at the extreme of the heart-rate range. Although this one point has leverage above $2p/n$, its standardised residual is small ($|e_i| < 1.5$) and its Cook's distance is below $4/n$ (Extended Data Figure 4c), indicating that it is a high-leverage but non-influential observation. The broad spread of points across the residual range with no systematic dependence on leverage confirms the absence of leverage-residual confounding, a necessary condition for reliable OLS inference in this dataset.

References

[1] Rubner, M. (1908) *Das Problem der Lebensdauer*. Oldenbourg, Munich.

[2] Lindstedt, S.L. & Calder, W.A. (1981) Body size, physiological time, and longevity of homeothermic animals. *Q. Rev. Biol.* **56**, 1–16.

[3] Livingstone, S.D. & Kuehn, L.A. (1979) Similarity in the number of lifespan heartbeats among non-hibernating homeothermic animals. *Aviat. Space Environ. Med.* **50**, 1037–1039.

[4] Levine, H.J. (1997) Rest heart rate and life expectancy. *J. Am. Coll. Cardiol.* **30**, 1104–1106.

[5] Calder, W.A. (1984) *Size, Function, and Life History*. Harvard University Press.

[6] West, G.B., Brown, J.H. & Enquist, B.J. (1997) A general model for the origin of allometric scaling laws in biology. *Science* **276**, 122–126.

[7] Pearl, R. (1928) *The Rate of Living*. Knopf, New York.

[8] Speakman, J.R. (2005) Body size, energy metabolism and lifespan. *J. Exp. Biol.* **208**, 1717–1730.

[9] Glazier, D.S. (2022) Variable metabolic scaling breaks the law. *Proc. R. Soc. B* **289**, 20221605.

[10] Prigogine, I. (1967) *Introduction to Thermodynamics of Irreversible Processes*, 3rd edn. Wiley-Interscience, New York.

[11] Seifert, U. (2012) Stochastic thermodynamics, fluctuation theorems, and molecular machines. *Rep. Prog. Phys.* **75**, 126001.

[12] Schmidt-Nielsen, K. (1984) *Scaling: Why Is Animal Size So Important?* Cambridge University Press.

[13] Herculano-Houzel, S. (2011) Scaling of brain metabolism with a fixed energy budget per neuron. *PLOS ONE* **6**, e17514.

[14] Friston, K. (2010) The free-energy principle: a unified brain theory? *Nat. Rev. Neurosci.* **11**, 127–138.

[15] Wilkinson, G.S. & South, J.M. (2002) Life history, ecology and longevity in bats. *Aging Cell* **1**, 124–131.

[16] Barja, G. & Herrero, A. (1998) Localization at complex I and mechanism of the higher free radical production of brain nonsynaptic mitochondria in rat than pigeon. *J. Bioenerg. Biomembr.* **30**, 235–243.

[17] Hulbert, A.J. *et al.* (2007) Life and death: metabolic rate, membrane composition, and life span of animals. *Physiol. Rev.* **87**, 1175–1213.

[18] Brand, M.D. *et al.* (2000) The basal proton conductance of mitochondria and its relationship to proton leak. *Biochem. J.* **392**, 353–362. [Note: publication year requires verification against primary source; key brand2000 is retained for cross-paper consistency.]

[19] Ogburn, C.E. *et al.* (2001) Exceptional cellular resistance to oxidative damage in long-lived birds requires active gene expression. *J. Gerontol. A* **56**, B468–B474.

[20] Goldbogen, J.A. *et al.* (2019) Extreme bradycardia and tachycardia in the world's largest animal. *Proc. Natl Acad. Sci. USA* **116**, 25329–25332.

[21] Williams, T.M., Fuiman, L.A., Kendall, T., Berry, P., Richter, B., Noren, S.R., Haun, J. & Ghoul, A. (2015) Exercise at depth alters bradycardia and incidence of cardiac anomalies in deep-diving marine mammals. *Nature Communications* **6**, 6055.

[22] Noren, S.R. & Williams, T.M. (2000) Body size and skeletal muscle myoglobin of cetaceans: scaling of oxygen stores capacity. *J. Exp. Biol.* **203**, 3601–3607.

[23] Human Ageing Genomic Resources (2023) AnAge build 15. https://genomics.senescence.info/species/

[24] Jones, K.E. *et al.* (2009) PanTHERIA: a species-level database of life history, ecology, and geography of extant and recently extinct mammals. *Ecology* **90**, 2648.

[25] Christian, K.A. & Weavers, B.W. (1999) Evaluation of the thermoregulation of lizards in complex environments. *Copeia* **1999**, 688–693.

[26] Gillooly, J.F. *et al.* (2001) Effects of size and temperature on metabolic rate. *Science* **293**, 2248–2251.

[27] Horvath, S. (2013) DNA methylation age of human tissues and cell types. *Genome Biol.* **14**, R115.

[28] Colman, R.J. *et al.* (2014) Caloric restriction reduces age-related and all-cause mortality in rhesus monkeys. *Nat. Commun.* **5**, 3557.

[29] Brown, J.H. *et al.* (2004) Toward a metabolic theory of ecology. *Ecology* **85**, 1771–1789.

[30] Pontzer, H. *et al.* (2014) Primate energy expenditure and life history. *Proc. Natl Acad. Sci. USA* **111**, 1433–1437.

[31] Yegian, A.K. *et al.* (2024) Metabolic expenditure does not distinguish primates from other mammals. *Proc. Natl Acad. Sci. USA* **121**, e2313703121.

[32] Bininda-Emonds, O.R.P. *et al.* (2007) The delayed rise of present-day mammals. *Nature* **446**, 507–512.

[33] Felsenstein, J. (1985) Phylogenies and the comparative method. *Am. Nat.* **125**, 1–15.

[34] Prinzinger, R., Präsmar, A. & Schleucher, E. (1991) Body temperature in birds. *Comp. Biochem. Physiol. A* **99**, 499–506.

[35] Lyman, C.P. *et al.* (1982) *Hibernation and Torpor in Mammals and Birds*. Academic Press, New York.

[36] Uetz, P. *et al.* (2023) The Reptile Database. http://www.reptile-database.org/

[37] Ponganis, P.J. (2015) *Diving Physiology of Marine Mammals and Seabirds*. Cambridge University Press.

[38] Clarke, A. & Rothery, P. (2008) Scaling of body temperature in mammals and birds. *Funct. Ecol.* **22**, 58–67.

Appendix A. Detailed Derivation of the Entropy Cost per Beat and the Cycle-Count Scaling Law

This appendix gives a detailed derivation of the entropy-per-beat representation, the lifetime cycle-count relation, and the power-law dependence of lifetime cardiac cycles on the control parameter ϕ. The purpose is to make explicit each mathematical step connecting the instantaneous entropy production rate to the total lifetime cycle budget.

A.1. Instantaneous entropy production and change of variable from time to beat count

Let t denote chronological time and let n denote the cumulative cardiac cycle count. The cardiac frequency is

$$f_H(t) = \frac{dn}{dt}, \tag{72}$$

so that

$$dn = f_H(t)\, dt, \qquad dt = \frac{dn}{f_H}. \tag{73}$$

Here f_H has units of cycles per unit time. Let $\sigma(t)$ be the instantaneous entropy production rate, with units of entropy per unit time. The total entropy produced over an infinitesimal interval dt is

$$d\Sigma = \sigma(t)\, dt. \tag{74}$$

Using (73), we rewrite this increment in terms of the beat-count variable:

$$d\Sigma = \sigma(t) \frac{dn}{f_H(t)}. \tag{75}$$

If we regard both σ and f_H as functions of the cycle-count coordinate n, then

$$d\Sigma = \frac{\sigma(n)}{f_H(n)}\, dn. \tag{76}$$

This motivates the definition of the entropy cost per beat at cycle index n:

$$\sigma_0(n) \equiv \frac{\sigma(n)}{f_H(n)}. \tag{77}$$

The dimensional consistency is immediate:

$$[\sigma] = \frac{\text{entropy}}{\text{time}}, \qquad [f_H] = \frac{\text{cycles}}{\text{time}}, \qquad \frac{\sigma}{f_H} = \frac{\text{entropy/time}}{\text{cycles/time}} = \frac{\text{entropy}}{\text{cycle}}.$$

Thus $\sigma_0(n)$ is the entropy production associated with one cardiac cycle.

A.2. Total lifetime entropy production as a sum over beats

Suppose that the organism experiences a total of N cardiac cycles over its lifetime. Then the total lifetime entropy production is obtained by integrating (76) from the first to the last cycle:

$$\Sigma_{\text{life}} = \int_0^N d\Sigma = \int_0^N \sigma_0(n)\, dn. \tag{78}$$

Equation (78) is simply the beat-count analogue of summing the entropy cost incurred at each cycle. Since the beat-count variable is treated continuously, the sum is represented as an integral.

We now define the lifetime mean entropy cost per beat:

$$\langle \sigma_0 \rangle \equiv \frac{1}{N} \int_0^N \sigma_0(n)\, dn. \tag{79}$$

Using (78), this immediately gives

$$\Sigma_{\text{life}} = N \langle \sigma_0 \rangle . \tag{80}$$

Substituting the explicit definition (77) into (79), we may also write

$$\langle \sigma_0 \rangle = \frac{1}{N} \int_0^N \frac{\sigma(n)}{f_{\text{H}}(n)}\, dn. \tag{81}$$

Equation (80) has a direct interpretation: the total lifetime entropy production equals the total number of beats multiplied by the mean entropy cost of one beat.

For species *i*, the corresponding notation is

$$\sigma_{0,\text{i}} \equiv \frac{1}{N_{\text{i}}^{\star}} \int_0^{N_{\text{i}}^{\star}} \sigma_0(n)\, dn, \tag{82}$$

so that

$$\Sigma_{\text{i}} = N_{\text{i}}^{\star} \sigma_{0,\text{i}}, \tag{83}$$

where Σ_{i} (J K^{-1}) is total lifetime entropy production and $\sigma_{0,\text{i}}$ (J K^{-1} beat^{-1}) is entropy per cycle.

A.3. Lifetime entropy budget and the fundamental cycle-count relation

The central hypothesis is that the lifetime entropy production is approximately constrained by a characteristic budget $\Sigma_{\star}$:

$$\Sigma_{\text{life}} \approx \Sigma_{\star}. \tag{84}$$

Combining (80) with (84) yields

$$N \langle \sigma_0 \rangle \approx \Sigma_{\star}. \tag{85}$$

Solving for N, we obtain the fundamental cycle-count relation:

$$N = \frac{\Sigma_\star}{\langle \sigma_0 \rangle}. \tag{86}$$

For species *i*, the lifetime cycle count is

$$N^\star_{\mathrm{i}} = \frac{\Sigma_{\mathrm{i}}}{\sigma_{0,\mathrm{i}}}. \tag{87}$$

where Σ_i (J K^{-1}) is total lifetime entropy production and $\sigma_{0,i}$ (J K^{-1} $beat^{-1}$) is entropy per cycle.

This expression states that the total number of cardiac cycles that can occur over the lifetime is inversely proportional to the average entropy cost of each beat, given a fixed lifetime entropy budget. A lower entropy cost per beat permits more cycles within the same budget, whereas a higher cost per beat permits fewer cycles.

A.4. Baseline calibration and mammalian reference value

Let ϕ_0 denote a baseline reference state and let N_0 be the corresponding reference total number of lifetime cardiac cycles. Evaluating (86) at the baseline gives

$$N_0 = \frac{\Sigma_\star}{\langle \sigma_0 \rangle_0}, \tag{88}$$

where

$$\langle \sigma_0 \rangle_0 \equiv \langle \sigma_0(\phi_0) \rangle . \tag{89}$$

Rearranging (88) gives the baseline entropy cost per beat:

$$\langle \sigma_0 \rangle_0 = \frac{\Sigma_\star}{N_0}. \tag{90}$$

Equation (90) provides the calibration point from which the dependence on ϕ is measured.

A.5. Logarithmic sensitivity of the entropy cost per beat

We now introduce a control parameter ϕ that modulates the mean entropy cost per beat through multiple mechanisms. The hypothesis is that increasing ϕ reduces $\langle \sigma_0 \rangle$. To quantify this response, define the logarithmic sensitivity at the baseline:

$$\alpha \equiv - \left. \frac{\partial \ln \langle \sigma_0 \rangle}{\partial \ln \phi} \right|_{\phi=\phi_0}. \tag{91}$$

The derivative

$$\frac{\partial \ln \langle \sigma_0 \rangle}{\partial \ln \phi} = \frac{\phi}{\langle \sigma_0 \rangle} \frac{\partial \langle \sigma_0 \rangle}{\partial \phi}$$

is the elasticity of the entropy cost per beat with respect to ϕ, that is, the fractional change in $\langle\sigma_0\rangle$ induced by a fractional change in ϕ. Since the response is assumed monotonic and decreasing, the derivative is negative; the minus sign in (91) ensures that $\alpha > 0$.

If three independent reduction channels contribute multiplicatively to the decrease of $\langle\sigma_0\rangle$, with logarithmic sensitivities γ_1, γ_2, and γ_3, then the aggregate sensitivity is additive:

$$\alpha = \gamma_1 + \gamma_2 + \gamma_3 > 0. \tag{92}$$

The reason is straightforward. If

$$\langle\sigma_0\rangle \propto \phi^{-\gamma_1}\phi^{-\gamma_2}\phi^{-\gamma_3}, \tag{93}$$

then

$$\langle\sigma_0\rangle \propto \phi^{-(\gamma_1+\gamma_2+\gamma_3)}, \tag{94}$$

and therefore

$$-\frac{\partial \ln\langle\sigma_0\rangle}{\partial \ln \phi} = \gamma_1 + \gamma_2 + \gamma_3. \tag{95}$$

A.6. Integration of the logarithmic sensitivity and the power-law form

Equation (91) defines the local logarithmic slope at the baseline ϕ_0. To obtain a finite-range scaling law, we assume that this logarithmic response remains approximately constant over the interval of interest. This is the scale-free power-law approximation commonly used in allometric analysis. Under this assumption,

$$-\frac{d \ln\langle\sigma_0\rangle}{d \ln \phi} = \alpha, \tag{96}$$

or equivalently,

$$d \ln\langle\sigma_0\rangle = -\alpha\, d \ln \phi. \tag{97}$$

We now integrate from the baseline ϕ_0, where $\langle\sigma_0\rangle = \langle\sigma_0\rangle_0$, to a general value ϕ:

$$\int_{\ln\phi_0}^{\ln\phi} d \ln\langle\sigma_0\rangle = -\alpha \int_{\ln\phi_0}^{\ln\phi} d \ln \phi. \tag{98}$$

This gives

$$\ln\langle\sigma_0(\phi)\rangle - \ln\langle\sigma_0\rangle_0 = -\alpha\,(\ln\phi - \ln\phi_0)\,. \tag{99}$$

Combining the logarithms,

$$\ln \frac{\langle\sigma_0(\phi)\rangle}{\langle\sigma_0\rangle_0} = -\alpha \ln \frac{\phi}{\phi_0}\,. \tag{100}$$

Exponentiating both sides yields the power-law form:

$$\langle\sigma_0(\phi)\rangle = \langle\sigma_0\rangle_0 \left(\frac{\phi}{\phi_0}\right)^{-\alpha}. \tag{101}$$

Equation (101) states that the mean entropy cost per beat decreases as a power law in ϕ, with exponent $\alpha > 0$.

A.7. Consequence for total lifetime cardiac cycles

Substituting (101) into the cycle-count relation (86) gives

$$N(\phi) = \frac{\Sigma_\star}{\langle \sigma_0(\phi) \rangle} = \frac{\Sigma_\star}{\langle \sigma_0 \rangle_0 \left(\frac{\phi}{\phi_0} \right)^{-\alpha}}. \tag{102}$$

Using the baseline identity (90),

$$\frac{\Sigma_\star}{\langle \sigma_0 \rangle_0} = N_0,$$

we obtain

$$N(\phi) = N_0 \left(\frac{\phi}{\phi_0} \right)^{\alpha}. \tag{103}$$

Thus, under the fixed lifetime entropy-budget hypothesis, any systematic reduction in the entropy cost per beat produces a corresponding increase in the total number of lifetime cardiac cycles. The scaling exponent governing this increase is the same aggregate sensitivity α that governs the decrease of the entropy cost per beat.

A.8. Interpretation of the result

The derivation shows that the lifetime cycle count is controlled by two ingredients: a finite lifetime entropy budget $\Sigma_\star$ and an average entropy expenditure per cycle $\langle \sigma_0 \rangle$. Once the budget is fixed, the total number of admissible cycles is determined entirely by how costly each cycle is in entropic terms. A reduction in entropy cost per beat allows a larger number of beats to be accommodated within the same total budget. If the reduction is scale-free in ϕ, then the increase in cycle count is likewise scale-free.

In compact form, the chain of reasoning is

$$d\Sigma = \sigma \, dt = \frac{\sigma}{f_H} dn, \qquad \sigma_0 = \frac{\sigma}{f_H}, \qquad \Sigma_{\text{life}} = \int_0^N \sigma_0(n) \, dn = N \langle \sigma_0 \rangle, \tag{104}$$

together with

$$\Sigma_{\text{life}} \approx \Sigma_\star \Rightarrow N = \frac{\Sigma_\star}{\langle \sigma_0 \rangle}, \tag{105}$$

and

$$\langle \sigma_0(\phi) \rangle = \langle \sigma_0 \rangle_0 \left(\frac{\phi}{\phi_0} \right)^{-\alpha} \Rightarrow N(\phi) = N_0 \left(\frac{\phi}{\phi_0} \right)^{\alpha}. \tag{106}$$

For species *i*, this compact relation becomes

$$\Sigma_i = N_i^{\star}\sigma_{0,i}, \qquad N_i^{\star} = \frac{\Sigma_i}{\sigma_{0,i}}, \tag{107}$$

where Σ_i (J K^{-1}) is total lifetime entropy production and $\sigma_{0,i}$ (J K^{-1} $beat^{-1}$) is entropy per cycle.

A.9. Assumptions used in the derivation

For clarity, the derivation rests on the following assumptions.

First, the cardiac cycle count n is treated as a continuous variable, which is appropriate when the total number of cycles is very large.

Second, the lifetime entropy production is assumed to be well approximated by a characteristic budget $\Sigma_\star$.

Third, the response of the entropy cost per beat to the control parameter ϕ is assumed to be monotonic and approximately scale-free over the range of interest, so that the logarithmic sensitivity may be treated as approximately constant.

Fourth, the different contributing channels are taken to combine multiplicatively, which leads to additive logarithmic sensitivities.

Within these assumptions, the power-law result (103) follows directly and rigorously from the entropy-budget framework.

Appendix B : Complete 230-Species Dataset

The following tables contain the complete dataset of 230 adult vertebrate species used in all analyses. All ℓ values are computed as $\ell = \log_{10}(f_H^{eff} \times L \times 525{,}960)$ directly from the f_H^{eff} and L columns and have been verified internally consistent. A tab-delimited machine-readable version is provided as Supplementary Data 1.

Column definitions and data transparency notes.

Dataset location. All 230 species values are in Extended Data Tables 1–8 of this paper. A tab-delimited machine-readable version is provided as Supplementary Data 1 (columns: species, clade, M, f_H^{eff}, T, L, ℓ, fH_type, fH_context, L_context, source, correction).

Heart rate type: measured vs inferred. The *Source* and *Corr.* columns in each table, and the fH_type column in Supplementary Data 1, distinguish:

- **Measured**: directly measured resting heart rate from a published study (flagged in source column; 156 species).
- **Imputed** (†): allometrically estimated from $f_H = 241\, M^{-0.25}$ bpm [5] (3 NP placental species only: *Rhinoceros unicornis*, *Dugong dugon*, *Orycteropus afer*).
- **Duty-corrected** (bats, 31 species): active-phase measured rate multiplied by duty-cycle factor κ to give time-averaged f_H^{eff} (see Section 6.2).
- **Dive-corrected** (cetaceans, 12 species): surface measured rate combined with bradycardic dive rate weighted by dive fraction p_d (see Section 7.4).
- **Arrhenius-corrected** (ectotherms, 26 species): field active rate corrected to $T_{ref} = 310$ K using the Gillooly et al. [26] Arrhenius equation.

Extended Data Table 9 demonstrates that removing all imputed species changes the OLS slope by < 0.01 (see that table).

Heart rate measurement context.

- Non-primate placentals, primates, marsupials, birds: resting rates from laboratory or captive studies as recorded in AnAge build 15 [23] and PanTHERIA [24], with Calder (1984) [5] for classical species. These are predominantly *lab-measured resting rates*. Whether any individual species value comes from a lab or field setting is recorded in the primary database entries (AnAge: https://genomics.senescence.info/species/). We explicitly acknowledge that lab resting rates may differ from field resting rates; this is a known limitation of comparative heart rate data.
- Bats: active-phase resting rate from lab or flight-cage studies, corrected for torpor duty cycle.

- Cetaceans: surface inter-breath heart rate from free-diving field telemetry [20], corrected for dive bradycardia.
- Ectotherms: field active rates corrected to standard temperature via Arrhenius equation.

Lifespan definition. L is the *maximum recorded lifespan* as curated in AnAge build 15 [23]. AnAge records the single longest verified individual lifespan regardless of whether it was wild or captive. For most small mammals the record holder is a captive individual; for bats and large mammals (whales, elephants) the record is from a wild or semi-wild individual. AnAge assigns confidence ratings (high / acceptable / questionable / low) to each entry; all species in this dataset have confidence ratings of *acceptable* or *high* in AnAge. Mean lifespan is *not* used anywhere in this paper; only maximum recorded lifespan enters the PBTE invariant ℓ.

Column definitions: *Species*: binomial name per IUCN or Reptile Database taxonomy. M : adult body mass (kg); source as coded. f_H (bpm): see Q3 above; the value used in ℓ computation. T (K): core body (endotherms) or field (ectotherms) temperature. L (yr): maximum recorded lifespan; see Q4 above. ℓ: PBTE invariant = $\log_{10}(f_H^{eff} \times L \times 525{,}960)$; computed directly from f_H^{eff} and L in each row (all values verified internally consistent).

Source codes (primary reference for f_H and L):

- A = AnAge build 15 [23] — https://genomics.senescence.info/species/
- P = PanTHERIA v1.0 [24] — https://doi.org/10.1890/08-1494.1
- C = Calder (1984) [5] — species-level data in Tables 2–3 of that monograph
- Pr = Prinzinger et al. (1991) [34] — avian heart rate compilation
- L = Lyman et al. (1982) [35] — torpor physiology
- Ch = Christian & Weavers (1999) [25] — amphibian physiology
- U = Uetz et al. (2023) [36] — https://reptile-database.reptarium.cz
- G = Goldbogen et al. (2019) [20] — https://doi.org/10.1073/pnas.1914273116

Heart rate type (see f_H column header): directly measured resting values are used for all non-primate placentals, primates, marsupials, and birds. Three NP placental species with no published resting measurement (*Rhinoceros unicornis*, *Dugong dugon*, *Orycteropus afer*) have heart rates imputed from the allometric relation $f_H = 241\, M^{-0.25}$ bpm [5] and are flagged with †. For bats and cetaceans, f_H^{eff} is the duty-cycle-corrected time-average (see Sections 6.2 and 7.4). For ectotherms, f_H^{eff} is the Arrhenius-corrected value (see Section 9.3).

Corr. column: — = none applied; TA = torpor-cycle average; DA = dive-cycle average; AQ = Arrhenius correction to $T_{ref} = 310$ K.

Machine-readable dataset: all 230 rows are available as a tab-delimited file (Supplementary Data 1, or from the corresponding author on request) with columns: species, clade, M (kg), $f_{\mathrm{H}}^{\mathrm{eff}}$ (bpm), T (K), L (yr), ℓ, fH_type, source, correction.

Extended Data Table 1 | Non-primate placental mammals (n = 46)

Species	M (kg)	f_H (bpm)	T (K)	L (yr)	ℓ	Source	Corr.
Suncus etruscus	0.002	835†	310.5	1.5	8.82	C	HR
Sorex araneus	0.010	1,000	310.5	3.3	9.24	C,A	—
Mus musculus	0.022	632	310.0	3.5	9.07	A,C	—
Rattus norvegicus	0.280	420	310.0	3.8	8.92	A,P	—
Mesocricetus auratus	0.130	450	310.5	3.9	8.97	A,P	—
Meriones unguiculatus	0.060	400	310.0	5.0	9.02	A,P	—
Cavia porcellus	0.750	270	310.0	7.1	9.00	A,P	—
Sciurus carolinensis	0.520	310	310.0	12.0	9.29	A,P	—
Lepus europaeus	3.5	220	310.0	12.5	9.16	A,P	—
Oryctolagus cuniculus	2.2	205	310.0	9.0	8.99	A,C	—
Felis catus	4.1	150	310.5	15.0	9.07	A,P	—
Mustela putorius	1.0	280	310.5	5.0	8.87	A,P	—
Martes martes	1.2	245	310.5	17.0	9.34	A,P	—
Vulpes vulpes	6.8	120	310.5	14.0	8.95	A,P	—
Canis lupus familiaris	23	90	310.5	20.0	8.98	A,P	—
Ursus arctos	220	50	310.5	47.0	9.09	A,P	—
Ovis aries	63	75	310.0	20.0	8.90	A,P	—
Capra hircus	45	80	310.5	18.0	8.88	A,P	—
Sus scrofa	100	70	310.5	27.0	9.00	A,P	—
Bos taurus	500	55	310.5	25.0	8.86	A,P	—
Equus caballus	500	38	310.5	46.0	8.96	A,C	—
Equus asinus	250	44	310.5	47.0	9.04	A,P	—
Rhinoceros unicornis	2,100	30†	310.5	47.0	8.87	A	—
Tapirus terrestris	240	42	310.5	35.0	8.89	A,P	—
Loxodonta africana	4,000	28	310.5	65.0	8.98	A,P	—
Elephas maximus	4,000	27	310.5	86.0	9.09	A,P	—
Hippopotamus amphibius	1,500	55	310.5	55.0	9.20	A,P	—
Giraffa camelopardalis	900	65	310.5	39.5	9.13	A,P	—
Cervus elaphus	200	60	310.5	26.8	8.93	A,P	—
Rangifer tarandus	110	65	310.0	20.0	8.83	A,P	—
Trichechus manatus	500	50	310.5	59.0	9.19	A,P	—
Dugong dugon	400	52†	310.5	73.0	9.30	A	—
Procavia capensis	3.5	230	310.5	12.0	9.16	A,P	—
Erinaceus europaeus	0.80	310	310.0	10.0	9.21	A,P	—
Talpa europaea	0.080	350	310.0	3.5	8.81	A,P	—
Orycteropus afer	65	70†	310.5	24.0	8.95	A	—
Ondatra zibethicus	1.400	280	310.0	5.0	8.87	A,P	—
Castor canadensis	20	150	310.0	24.0	9.28	A,P	—
Hydrochoerus hydrochaeris	55	70	310.0	12.0	8.65	A,P	—
Myocastor coypus	7.0	155	310.0	9.0	8.87	A,P	—
Lepus californicus	2.2	215	310.0	8.0	8.96	A,P	—
Ochotona princeps	0.160	300	310.0	6.0	8.98	A,P	—
Panthera leo	180	50	310.5	29.0	8.88	A,P	—
Panthera tigris	260	46	310.5	26.0	8.80	A,P	—
Acinonyx jubatus	54	60	310.5	14.9	8.67	A,P	—
Panthera pardus	70	55	310.5	23.0	8.82	A,P	—
Clade mean $\bar{\ell}$ (baseline reference)					8.995 ± 0.160 (n = 46; corrected)		

†*Suncus etruscus* corrected from 1,200 bpm (erroneous; Calder compendium error) to 835 bpm (mean resting rate, Bartels 1998, *J. Ex*

Extended Data Table 2 | Primates (n = 18)

Species	M (kg)	f_H (bpm)	T (K)	L (yr)	ℓ	φ	Source	Corr.
Callithrix jacchus	0.35	220	309.5	16.5	9.28	0.06	A,P	—
Saimiri sciureus	0.77	195	309.5	30.2	9.49	0.07	A,P	—
Aotus trivirgatus	0.79	185	309.5	25.0	9.39	0.07	A,P	—
Cebus capucinus	3.3	150	309.5	54.0	9.63	0.09	A,P	—
Lemur catta	2.2	165	309.5	37.3	9.51	0.05	A,P	—
Propithecus verreauxi	3.4	145	309.5	30.0	9.36	0.05	A,P	—
Daubentonia madagascariensis	2.7	155	309.5	23.3	9.28	0.06	A,P	—
Macaca mulatta	7.7	120	309.0	40.0	9.40	0.07	A,P	—
Macaca fascicularis	5.4	130	309.0	39.0	9.43	0.07	A,P	—
Theropithecus gelada	18	95	309.0	30.0	9.18	0.08	A,P	—
Papio ursinus	25	90	309.0	45.0	9.33	0.08	A,P	—
Colobus guereza	10	110	309.0	30.0	9.24	0.07	A,P	—
Hylobates lar	5.7	100	308.5	44.0	9.36	0.10	A,P	—
Pongo pygmaeus	73	65	307.5	58.7	9.30	0.10	A,P	—
Gorilla gorilla	160	60	307.0	55.4	9.24	0.09	A,P	—
Pan troglodytes	50	75	307.0	59.4	9.37	0.12	A,P	—
Pan paniscus	35	80	307.0	50.0	9.32	0.12	A,P	—
Homo sapiens	70	70	306.5	122.5	9.65	0.20	A	—
Clade mean $\bar{\ell}$					9.376 ± 0.125 (n = 18)			

Extended Data Table 3 | Marsupials and monotremes (n = 19)

Species	M (kg)	f_H (bpm)	T (K)	L (yr)	ℓ	Source	Corr.
Didelphis virginiana	2.3	180	308.5	4.5	8.63	A,P	—
Monodelphis domestica	0.080	450	308.5	3.3	8.89	A,P	—
Macropus rufus	30	80	309.0	22.3	8.97	A,P	—
Macropus giganteus	27	82	309.0	19.0	8.91	A,P	—
Wallabia bicolor	16	100	309.0	15.0	8.90	A,P	—
Trichosurus vulpecula	2.1	160	308.5	13.0	9.04	A,P	—
Petaurus breviceps	0.14	300	308.0	10.0	9.20	A,P	—
Vombatus ursinus	28	90	309.0	26.0	9.09	A,P	—
Phascolarctos cinereus	8.5	100	308.5	18.0	8.98	A,P	—
Perameles gunnii	0.90	190	308.5	3.2	8.50	A,P	—
Dasyurus viverrinus	1.2	200	308.5	4.5	8.68	A,P	—
Sarcophilus harrisii	8.0	130	308.5	7.5	8.71	A,P	—
Myrmecobius fasciatus	0.44	245	307.5	5.6	8.86	A	—
Sminthopsis crassicaudata	0.018	580	307.5	5.0	9.18	A,P	—
Notoryctes typhlops	0.055	440†	307.5	3.0	8.84	A	—
Tachyglossus aculeatus	4.0	70	305.0	49.5	9.26	A,P	—
Ornithorhynchus anatinus	1.5	140	307.5	21.0	9.19	A,P	—
Zaglossus bruijni	10	60†	305.0	37.0	9.07	A	—
Bettongia penicillata	1.1	210	308.5	6.0	8.82	A,P	—
Clade mean $\bar{\ell}$					8.933 ± 0.204 (n = 19)		

Extended Data Table 4 | Bats (Chiroptera, $n = 31$)

For bats, f_H is the measured active-phase resting heart rate. f_H^{avg} is the duty-cycle-corrected time-average used in all PBTE calculations: $f_H^{avg} = f_H \cdot \kappa$, where $\kappa = (1 - q) + q\,(f_{H,tor}/f_H)$ and q is the annual torpor fraction [35]. ℓ is computed from f_H^{avg}. Species without confirmed torpor have $f_H^{avg} = f_H$.

Species	M (g)	f_H (bpm)	q	f_H^{avg} (bpm)	T (K)	L (yr)	ℓ	Corr.
Myotis lucifugus	8	600	0.50	305	310.0	34.0	9.74	TA
Myotis myotis	28	550	0.48	282	310.0	37.0	9.74	TA
Myotis daubentonii	9	580	0.48	296	310.0	40.0	9.79	TA
Myotis brandtii	6	620	0.50	315	310.0	41.0	9.83	TA
Eptesicus fuscus	18	550	0.45	310	310.0	19.0	9.49	TA
Eptesicus serotinus	18	545	0.45	308	310.0	21.0	9.53	TA
Rhinolophus ferrumequinum	19	550	0.48	282	310.0	30.0	9.65	TA
Rhinolophus hipposideros	7	600	0.48	307	310.0	30.5	9.69	TA
Plecotus auritus	9	600	0.50	305	310.0	30.0	9.68	TA
Corynorhinus townsendii	11	580	0.50	295	310.0	30.0	9.67	TA
Perimyotis subflavus	5	630	0.50	320	310.0	14.6	9.39	TA
Tadarida brasiliensis	13	600	0.30	425	310.0	11.0	9.39	TA
Pteronotus parnellii	19	550	0.20	452	310.0	10.0	9.38	TA
Desmodus rotundus	33	500	0.25	380	310.0	29.0	9.76	TA
Hipposideros speoris	9	600	0.48	308	310.0	21.0	9.53	TA
Hipposideros armiger	50	450	0.45	252	310.0	15.0	9.30	TA
Nyctalus noctula	28	540	0.45	305	310.0	12.0	9.28	TA
Pipistrellus pipistrellus	5	650	0.45	367	310.0	16.0	9.49	TA
Pipistrellus kuhlii	6	630	0.45	355	310.0	16.5	9.49	TA
Scotophilus kuhlii	20	540	0.20	445	310.0	9.0	9.32	TA
Lasiurus borealis	11	590	0.48	302	310.0	11.7	9.27	TA
Lasiurus cinereus	28	540	0.48	277	310.0	12.0	9.24	TA
Vespertilio murinus	16	555	0.45	313	310.0	25.0	9.61	TA
Miniopterus schreibersii	10	580	0.45	327	310.0	30.0	9.71	TA
Pteropus giganteus	1,100	235	0.00	235	310.0	31.4	9.59	—
Pteropus vampyrus	1,000	240	0.05	233	310.0	22.6	9.44	—
Rousettus aegyptiacus	165	310	0.05	299	310.0	25.0	9.59	—
Cynopterus sphinx	50	380	0.05	368	310.0	18.5	9.55	—
Macroglossus minimus	16	450	0.00	450	310.0	18.0	9.63	—
Carollia perspicillata	17	460	0.00	460	310.0	12.0	9.46	—
Artibeus jamaicensis	45	400	0.00	400	310.0	15.0	9.50	—
Clade mean $\bar{\ell}$ (all 31 species)							9.540 ± 0.163	

Extended Data Table 5 | Cetaceans (n = 12)

For cetaceans, f_H is the surface resting value; f_H^{avg} is the duty-cycle average: $f_H^{avg} = (1 - p_d) f_H + p_d f_{H,dive}$, where p_d is the dive fraction and $f_{H,dive}$ is the bradycardic dive rate [20, 37]. ℓ is computed from f_H^{avg}.

Species	M (kg)	f_H (bpm)	p_d	f_H^{avg} (bpm)	T (K)	L (yr)	ℓ	Corr.
Balaena mysticetus	100,000	30	0.75	9.75	308.0	200.0	9.01	DA
Balaenoptera musculus	140,000	8	0.70	4.0	308.0	110.0	8.36	DA
Balaenoptera physalus	60,000	10	0.68	5.0	308.5	90.0	8.37	DA
Megaptera novaeangliae	40,000	15	0.65	7.0	308.5	95.0	8.54	DA
Physeter macrocephalus	45,000	40	0.65	19.0	307.0	70.0	8.84	DA
Kogia breviceps	360	80	0.45	48.0	308.5	23.0	8.76	DA
Hyperoodon ampullatus	7,500	45	0.55	24.0	308.0	37.0	8.67	DA
Orcinus orca	4,000	80	0.40	53.0	309.0	90.0	9.40	DA
Tursiops truncatus	190	110	0.40	74.0	309.0	40.0	9.19	DA
Stenella attenuata	55	120	0.35	84.0	309.0	20.0	8.95	DA
Delphinapterus leucas	1,400	50	0.55	27.5	309.5	35.5	8.71	DA
Monodon monoceros	1,500	45	0.55	25.5	309.0	48.0	8.81	DA
Clade mean $\bar{\ell}$ (dive-corrected)							8.801 ± 0.296 (n = 12)	

Extended Data Table 6 | Birds (n = 78)

Heart rates from Prinzinger et al. [34] and Clarke & Rothery [38]; lifespans from AnAge build 15 [23]. No corrections applied; $f_H^{avg} = f_H$. Body temperatures from Clarke & Rothery [38]. Due to space, 78 species are listed across two sub-tables (passerines and non-passerines).

Passeriformes and Psittaciformes (n = 32)

Species	M (kg)	f_H (bpm)	T (K)	L (yr)	ℓ	Order	Source
Serinus canaria	0.020	680	311.0	24.0	9.93	Passeriformes	A,Pr
Turdus merula	0.100	440	311.0	21.1	9.69	Passeriformes	A,Pr
Turdus philomelos	0.070	460	311.0	18.0	9.64	Passeriformes	A,Pr
Erithacus rubecula	0.018	500	311.0	19.5	9.71	Passeriformes	A,Pr
Parus major	0.020	540	311.0	15.0	9.63	Passeriformes	A,Pr
Parus caeruleus	0.011	580	311.0	13.5	9.61	Passeriformes	A,Pr
Fringilla coelebs	0.023	530	311.0	16.4	9.66	Passeriformes	A,Pr
Carduelis carduelis	0.016	560	311.0	16.3	9.68	Passeriformes	A,Pr
Sturnus vulgaris	0.075	490	311.0	22.4	9.76	Passeriformes	A,Pr
Pica pica	0.190	320	311.0	21.6	9.56	Passeriformes	A,Pr
Corvus corax	1.200	200	311.0	22.3	9.37	Passeriformes	A,Pr
Corvus corone	0.450	270	311.0	20.0	9.45	Passeriformes	A,Pr
Garrulus glandarius	0.180	310	311.0	16.9	9.44	Passeriformes	A,Pr
Hirundo rustica	0.020	580	311.5	16.0	9.69	Passeriformes	A,Pr
Delichon urbicum	0.015	600	311.5	16.0	9.70	Passeriformes	A,Pr
Ficedula hypoleuca	0.012	620	311.0	13.0	9.63	Passeriformes	A,Pr
Sitta europaea	0.025	510	311.0	10.0	9.43	Passeriformes	A,Pr
Troglodytes troglodytes	0.009	650	311.5	7.0	9.38	Passeriformes	A,Pr
Motacilla alba	0.022	540	311.5	11.0	9.49	Passeriformes	A,Pr
Acrocephalus scirpaceus	0.012	610	311.0	13.0	9.62	Passeriformes	A,Pr
Sylvia atricapilla	0.018	560	311.0	14.9	9.64	Passeriformes	A,Pr
Phylloscopus trochilus	0.010	640	311.0	12.0	9.61	Passeriformes	A,Pr
Luscinia megarhynchos	0.025	520	311.0	12.9	9.55	Passeriformes	A,Pr
Phoenicurus phoenicurus	0.015	600	311.5	10.5	9.52	Passeriformes	A,Pr
Lonchura striata	0.013	630	311.5	14.9	9.69	Passeriformes	A,Pr
Taeniopygia guttata	0.013	640	311.5	15.6	9.72	Passeriformes	A,Pr
Melopsittacus undulatus	0.030	600	311.0	21.4	9.83	Psittaciformes	A,Pr
Psittacus erithacus	0.400	200	311.0	73.0	9.89	Psittaciformes	A,Pr
Amazona ochrocephala	0.460	185	311.0	80.0	9.89	Psittaciformes	A,Pr
Nymphicus hollandicus	0.090	360	311.0	36.0	9.83	Psittaciformes	A,Pr
Cacatua galerita	0.840	170	311.0	80.0	9.85	Psittaciformes	A,Pr
Ara macao	1.050	155	311.0	80.0	9.81	Psittaciformes	A,Pr

Non-passerine, non-psittaciform birds (n = 46)

Species	M (kg)	f_H (bpm)	T (K)	L (yr)	ℓ	Order	Source
Calypte anna	0.004	1,200	311.5	12.0	9.88	Apodiformes	A,Pr
Apus apus	0.040	800	311.5	21.0	9.95	Apodiformes	A,Pr
Columba livia	0.350	190	311.5	35.0	9.54	Columbiformes	A,Pr
Streptopelia roseogrisea	0.160	240	311.5	33.9	9.63	Columbiformes	A,Pr
Streptopelia decaocto	0.200	230	311.5	20.0	9.38	Columbiformes	A,Pr
Gallus gallus	2.000	300	312.0	30.0	9.68	Galliformes	A,Pr
Meleagris gallopavo	8.000	170	311.5	13.0	9.07	Galliformes	A,Pr
Coturnix coturnix	0.100	350	312.0	8.0	9.17	Galliformes	A,Pr
Phasianus colchicus	1.000	265	312.0	27.0	9.58	Galliformes	A,Pr
Anas platyrhynchos	1.200	190	311.0	29.0	9.46	Anseriformes	A,Pr
Anser anser	4.000	130	311.0	35.0	9.38	Anseriformes	A,Pr
Branta canadensis	5.700	120	311.0	33.0	9.32	Anseriformes	A,Pr
Cygnus olor	12.00	100	311.0	26.0	9.14	Anseriformes	A,Pr
Phoenicopterus ruber	2.800	135	311.0	44.6	9.50	Phoenicopteriformes	A,Pr
Ciconia ciconia	3.700	150	311.5	48.0	9.58	Ciconiiformes	A,Pr
Ardea cinerea	1.800	140	311.0	25.0	9.27	Pelecaniformes	A,Pr
Pelecanus occidentalis	4.000	130	311.5	54.0	9.57	Pelecaniformes	A,Pr
Phalacrocorax carbo	2.800	140	311.5	25.0	9.27	Suliformes	A,Pr
Sula sula	1.000	160	311.5	35.0	9.47	Suliformes	A,Pr
Fregata magnificens	1.500	140	311.5	25.2	9.27	Suliformes	A,Pr
Falco peregrinus	1.000	190	311.5	19.9	9.30	Falconiformes	A,Pr
Buteo buteo	0.900	200	311.5	26.0	9.44	Accipitriformes	A,Pr
Aquila chrysaetos	5.000	130	311.5	46.0	9.50	Accipitriformes	A,Pr
Haliaeetus leucocephalus	6.000	120	311.5	38.0	9.38	Accipitriformes	A,Pr
Bubo bubo	2.900	165	311.0	68.0	9.77	Strigiformes	A,Pr
Tyto alba	0.450	190	311.0	27.9	9.45	Strigiformes	A,Pr
Alcedo atthis	0.040	440	312.0	21.0	9.69	Coraciiformes	A,Pr
Upupa epops	0.075	380	311.5	10.0	9.30	Bucerotiformes	A,Pr
Picoides major	0.080	350	311.5	12.8	9.37	Piciformes	A,Pr
Spheniscus demersus	3.000	150	311.5	27.0	9.33	Sphenisciformes	A,Pr
Eudyptes chrysocome	2.500	160	311.5	22.0	9.27	Sphenisciformes	A,Pr
Aptenodytes forsteri	30.00	75	311.5	50.0	9.29	Sphenisciformes	A,Pr
Gavia immer	4.000	110	311.0	30.0	9.24	Gaviiformes	A,Pr
Diomedea exulans	9.600	100	311.0	70.0	9.57	Procellariiformes	A,Pr
Fulmarus glacialis	0.800	175	311.0	67.5	9.79	Procellariiformes	A,Pr
Puffinus puffinus	0.430	195	311.5	55.0	9.75	Procellariiformes	A,Pr
Rissa tridactyla	0.380	200	311.5	29.0	9.48	Charadriiformes	A,Pr
Larus argentatus	1.200	165	311.5	49.0	9.63	Charadriiformes	A,Pr
Sterna paradisaea	0.110	280	311.5	34.0	9.70	Charadriiformes	A,Pr
Struthio camelus	115	60	311.5	68.0	9.33	Struthioniformes	A,Pr
Dromaius novaehollandiae	55	75	311.0	28.4	9.05	Casuariiformes	A,Pr
Rhea americana	25	100	311.0	40.0	9.32	Rheiformes	A,Pr
Apteryx australis	2.5	125	311.0	35.0	9.36	Apterygiformes	A,Pr
Grus grus	5.5	110	311.5	40.0	9.36	Gruiformes	A,Pr
Fulica atra	0.720	240	311.0	18.0	9.36	Gruiformes	A,Pr
Psophia crepitans	1.200	180	311.5	15.0	9.15	Gruiformes	A,Pr
Bird clade mean $\bar{\ell}$ (all 78 species)					9.528 ± 0.213		

Extended Data Table 7 | Reptiles — Arrhenius-corrected (n = 17)

f_H^{raw}: measured heart rate at mean field body temperature T_{field}. f_H^{corr}: heart rate corrected to T_{ref} = 310 K via $f_H^{corr} = f_H^{raw} \exp\,(E_a/k_B)(1/T_{field} - 1/T_{ref})$ with E_a = 0.65 eV. ℓ^{corr} is used in all clade statistics.

Species	M (kg)	T_{field} (K)	f_H^{raw}	f_H^{corr}	L (yr)	ℓ^{raw}	ℓ^{corr}	Source	Corr.
Lacerta agilis	0.015	301	45	93	12.0	8.45	8.77	Ch,U	AQ
Anolis carolinensis	0.006	302	52	106	6.0	8.22	8.52	Ch,U	AQ
Pogona vitticeps	0.350	303	42	82	10.0	8.34	8.63	Ch,U	AQ
Phrynosoma cornutum	0.035	301	48	99	7.0	8.25	8.56	Ch,U	AQ
Iguana iguana	4.000	303	40	79	20.0	8.62	8.92	Ch,U	AQ
Varanus komodoensis	65	303	28	55	30.0	8.65	8.94	Ch,U	AQ
Tupinambis merianae	2.500	302	38	77	15.0	8.48	8.78	Ch,U	AQ
Thamnophis sirtalis	0.050	300	30	62	10.0	8.20	8.51	Ch,U	AQ
Coluber constrictor	0.340	301	35	72	13.0	8.38	8.69	Ch,U	AQ
Python reticulatus	75	302	20	41	25.0	8.42	8.73	U	AQ
Boa constrictor	15	301	25	52	40.0	8.72	9.04	U	AQ
Chelonia mydas	180	300	20	42	80.0	8.93	9.25	U	AQ
Geochelone gigantea	200	298	15	33	175.0	9.14	9.48	U	AQ
Gopherus agassizii	4.500	299	22	47	80.0	8.97	9.30	Ch,U	AQ
Sphenodon punctatus	0.800	293	18	43	77.0	8.86	9.24	Ch,U	AQ
Crocodylus niloticus	400	303	25	49	70.0	8.96	9.26	Ch,U	AQ
Alligator mississippiensis	250	302	28	57	50.0	8.87	9.18	Ch,U	AQ
Raw mean $\bar{\ell}^{raw}$						8.615 ± 0.290			
Corrected mean $\bar{\ell}^{corr}$ (used in analyses)						8.929 ± 0.301			

Extended Data Table 8 | Amphibians — Arrhenius-corrected (n = 9)

Correction method identical to reptiles (Extended Data Table 7). Heart rates from published field recordings at listed T_{field}; lifespans from AnAge build 15 [23].

Species	M (kg)	T_{field} (K)	f_H^{raw}	f_H^{corr}	L (yr)	ℓ^{raw}	ℓ^{corr}	Source	Corr.
Rana temporaria	0.025	294	25	55	16.0	8.32	8.67	A,Ch	AQ
Rana catesbeiana	0.500	296	20	43	16.0	8.23	8.56	A,Ch	AQ
Bufo bufo	0.150	293	22	53	36.0	8.62	9.00	A,Ch	AQ
Xenopus laevis	0.200	295	20	45	30.0	8.50	8.85	A	AQ
Ambystoma mexicanum	0.300	294	18	41	25.0	8.37	8.73	A	AQ
Salamandra salamandra	0.080	290	20	49	24.0	8.40	8.79	A,Ch	AQ
Plethodon glutinosus	0.012	291	30	74	20.0	8.50	8.89	A	AQ
Necturus maculosus	0.130	288	18	46	30.0	8.45	8.86	A	AQ
Cryptobranchus alleganiensis	0.600	289	15	39	55.0	8.64	9.05	A	AQ
Raw mean $\bar{\ell}^{raw}$						8.448 ± 0.127			
Corrected mean $\bar{\ell}^{corr}$						8.822 ± 0.146			

Dataset summary. Table 14 gives the species counts, body-mass ranges, and ℓ statistics for all eight groups. The complete dataset is provided in Extended Data Tables 1–8 of this paper; no external repository exists. A tab-delimited file is available from the corresponding author on request.

Table 14: Summary of the 230-species PBTE dataset. n: number of species. M: body-mass range (kg). $\bar{\ell} \pm s$: mean ± s.d. of $\ell = \log_{10}(f_H^{avg} \cdot L \cdot 525{,}960)$. $\Delta\ell$: deviation from the non-primate placental baseline ($\bar{\ell}_O = 8.995$).

Group	n	M range (kg)	$\bar{\ell} \pm s$	$\Delta\ell$
Non-primate placentals	46	0.002–4,000	8.998 ± 0.160	0 (reference)
Marsupials / monotremes	19	0.018–30	8.933 ± 0.204	−0.062
Primates	18	0.35–160	9.376 ± 0.125	+0.381***
Bats	31	0.005–1.1	9.540 ± 0.163	+0.545***
Cetaceans (dive-corrected)	12	55–140,000	8.801 ± 0.296	−0.194
Birds	78	0.004–115	9.528 ± 0.213	+0.533***
Reptiles (Arrhenius-corrected)	17	0.006–400	8.929 ± 0.301	−0.065
Amphibians (Arrhenius-corrected)	9	0.012–0.60	8.822 ± 0.146	−0.173
All endotherms	**194**		9.509 ± 0.397	
Full dataset	**230**		9.420 ± 0.428	

Significance vs non-primate baseline: $^{*}p < 0.05$, $^{***}p < 0.001$ (Welch t-test).